NASA TECHNICAL
MEMORANDUM

NASA TM X-3519

NASA TM X-3519

ACOUSTIC TESTS OF AUGMENTOR WING MODEL

Jack H. Goodykoontz
Lewis Research Center
Cleveland, Ohio 44135

NATIONAL AERONAUTICS AND SPACE ADMINISTRATION • WASHINGTON, D. C. • APRIL 1977

1. Report No. NASA TM X-3519	2. Government Accession No.	3. Recipient's Catalog No.

4. Title and Subtitle ACOUSTIC TESTS OF AUGMENTOR WING MODEL	5. Report Date April 1977
	6. Performing Organization Code
7. Author(s) Jack H. Goodykoontz	8. Performing Organization Report No. E-8923
9. Performing Organization Name and Address Lewis Research Center National Aeronautics and Space Administration Cleveland, Ohio 44135	10. Work Unit No. 505-05
	11. Contract or Grant No.
12. Sponsoring Agency Name and Address National Aeronautics and Space Administration Washington, D.C. 20546	13. Type of Report and Period Covered Technical Memorandum
	14. Sponsoring Agency Code

15. Supplementary Notes

16. Abstract

Acoustic and aerodynamic data were obtained for a full-scale section of an augmentor wing. Novel features of the design included a single-row, multielement nozzle array and acoustically tuned panels placed on the interior surfaces of the augmentor. When the data were extrapolated to a 91 000-kilogram aircraft, the calculated sideline perceived noise levels were approximately the same for either the takeoff or approach condition. For example, for an aircraft at 76.2 meters altitude, the 152.4-meter-sideline perceived noise levels for a standard day were 98 PNdB for takeoff and 97 PNdB for approach.

17. Key Words (Suggested by Author(s)) Acoustics; Aerodynamic noise; Aircraft noise; Jet aircraft noise; Lift augmentation; Short takeoff aircraft; Noise (sound); Wing flaps	18. Distribution Statement Unclassified - unlimited STAR Category 02

19. Security Classif. (of this report) Unclassified	20. Security Classif. (of this page) Unclassified	21. No. of Pages 54	22. Price* A04

* For sale by the National Technical Information Service, Springfield, Virginia 22161

ACOUSTIC TESTS OF AUGMENTOR WING MODEL

by Jack H. Goodykoontz

Lewis Research Center

SUMMARY

Acoustic and aerodynamic data were obtained for a full-scale section of an augmentor wing. The model configuration represents the latest development in noise suppression technology applied to this type of lift augmentation system. Novel features of the design included a single-row, multielement-lobe nozzle array and acoustically tuned panels placed on the interior surfaces of the augmentor.

The purpose of the work was to investigate scaling effects by comparing the large-scale-model acoustic data with data obtained under NASA contract on small scale models. In addition, a general acoustic evaluation of the hardware was performed; in particular, the effect of the acoustic panels was investigated.

Applying the scaling laws to the small-scale-model data predicted the large-scale-model noise levels only for the approach configuration. The procedure did not predict takeoff noise levels, possibly as a result of the lack of agreement in the flow conditions at the augmentor exit for the two models.

The effect of the acoustic panels, as compared with the hard-wall case, was to reduce the noise levels more for the landing configuration than for the takeoff configuration. However, when the data were extrapolated to a 91 000-kilogram aircraft, the calculated sideline perceived noise levels were approximately the same for either the takeoff or approach condition. For example, for an aircraft at 76.2 meters altitude, the 152.4-meter-sideline perceived noise levels for a standard day were 98 PNdB for takeoff and 97 PNdB for approach.

INTRODUCTION

The augmentor-wing powered lift system (fig. 1) appears to be more amenable to noise suppression techniques than other lift augmentation systems such as the externally blown flap and internally blown jet flap. Suppression benefits can be realized not only by ordinary shielding, but also, since the nozzle flow passes through a channel, by applying acoustic panels on the interior walls of the ejector. For example, a cursory examination of the effect of acoustic linings reported in reference 1 showed about a 5-decibel reduction in the spectral peak noise level when compared with the hardwall case.

Small-scale-model tests (ref. 2) showed promise that a 91 000-kilogram (200 000 lb) STOL aircraft using the augmentor wing configuration would meet the 152.4-meter (500-ft) sideline noise goal of 95 PNdB. The results were based on small-scale screening tests of a variety of nozzle types. Optimum performance, in terms of aerodynamics and noise suppression, in addition to weight and installation advantages, was attained by using a unique single-row multielement nozzle with the exit periphery of each element corrugated. The inner walls of the ejector were also lined with multilayer acoustic panels tuned to the frequency at which the peak noise level occurred.

As a result of the conclusions obtained from these small-scale-model tests, NASA contracted for the manufacture of a large scale model of the optimum augmentor wing configuration of reference 2. The need for test results from a large scale model was based on the uncertainty in the large extrapolations necessary in scaling the small-scale-model acoustic results to full size (91 000-kg aircraft).

This report presents experimental acoustic results obtained from the large-scale augmentor wing model and compares the results with small-scale-model data in order to validate scaling laws. The data are presented with the model in an optimum static thrust augmentation configuration. That is, the relative positions of nozzle to augmentor, both axially and laterally, and the ejector diffusion angle were set to simulate the conditions at which static thrust is maximum. These conditions were determined from the small-scale static thrust measurements of reference 2.

The large scale model was sized, in the spanwise direction, so that the required airflow rate to give a maximum nozzle pressure ratio of 2.6 was within the airflow capability at the Lewis Research Center. The nozzle height and augmentor chord length were the same as those anticipated to be used on a 91 000-kilogram aircraft. Nozzle pressure ratio was varied from 1.6 to 2.6, with the airflow rate ranging from approximately 20 to 36 kilograms per second. All tests were conducted with unheated air (280 to 300 K).

Test equipment was built and measurements were made in the U.S. customary system of units. The values were converted to the SI system of units for this report.

APPARATUS AND PROCEDURE

The experimental facility, shown in figure 2, consisted of an airflow system, the nozzle, and the augmentor. The following sections describe these items as well as the instrumentation and test procedure.

Airflow System

The airflow system is shown schematically in figure 3. Dry unheated air (280 to 300 K) was supplied to a 40-centimeter-diameter gate shutoff valve through an underground pipeline from the Center's air supply system (1 MN/m^2 gage max.). Airflow rate and nozzle pressure ratio (nozzle total pressure divided by local atmospheric pressure) were set by adjusting a 25-centimeter-diameter, butterfly flow control valve.

A muffler system in the airflow line downstream of the flow control valve attenuated internal noise caused primarily by the flow control valve. Essentially, the muffler system consisted of perforated plates and dissipative mufflers. The perforated plates were located immediately downstream of the flow control valve (40 percent open area) and at the entrance and exit of the first dissipative muffler (20 percent open area). Both the first and second mufflers were sections of pipe that housed crossed splitter plates oriented at right angles to one another so that the flow was divided into four channels. All internal surfaces of the muffler pipes and all surfaces of the splitter plates were covered with acoustic absorbent material. The second muffler was located downstream of the last 45° elbow in the airflow line to take advantage of the reflections caused by turning the flow. A third muffler was located directly beneath the nozzle feed plenum of the test model. Again, it consisted of a section of pipe lined internally with acoustic absorbent material and baffled internally so that there was no direct line of sight between the flow inlet and outlet of the muffler.

The nozzle feed plenum was a 76-centimeter-diameter pipe that extended the entire length of the test nozzle span. The discharge from the plenum entered a nozzle extension that was merely a transition section to interface the plenum and the test nozzle. Splitter plates were mounted at various spanwise locations inside the nozzle extension to promote good flow distribution to the nozzle. A general arrangement of the nozzle inlet plenum, the nozzle extension, and the corrugated-lobe nozzle is shown in the schematic drawing of figure 4(a).

Test Nozzle

The corrugated-lobe test nozzle (fig. 4(a)) consisted of 12 elements (or lobes) at a spanwise spacing of 15.87 centimeters to give an overall nozzle span of 174.6 centimeters (from centerline to centerline of the outermost lobes). Total exit flow area of the nozzle array was 626.8 square centimeters, which corresponds to an equivalent diameter D_{et} of 28.25 centimeters (all symbols defined in appendix A). Array area ratio, or the ratio of the total area bounded by the nozzle exits to the nozzle exit flow area, was 7.28. The flow coefficient (ratio of actual flow rate to ideal flow rate) varied from 0.88 to 0.92 over the range of test conditions.

Each individual lobe (fig. 4(b)) was convergent in cross-sectional area from inlet to outlet, with the exit plane of the lobe canted 20° with respect to the inlet plane. Canting of the exit plane reduced the flow turning angle for large angles between the augmentor (or ejector) axis and the wing chord plane. Splitter plates were installed at the exit of each lobe to eliminate screech tones. The corrugated periphery was incorporated to increase the ratio of jet perimeter to jet area. This provided a larger jet mixing surface, which, in effect, suppressed the noise generated by the individual lobes in the corrugated-lobe nozzle relative to a plane-lobe nozzle (ref. 2). The nozzle is shown in figures 4(c) and (d).

Augmentor

The augmentor (fig. 5(a)) consists of a flap (lower airfoil), a shroud (upper airfoil), an intake door, and two end plates (not shown). The flap and shroud had the same chord length and were sized to simulate an augmentor that would be used for an aircraft in the 91 000-kilogram range. The model had a span of 1.91 meters and was mounted on a stand with the spanwise direction vertical. Distance from center span to ground level was 4.1 meters (fig. 3). The profile shape of the wing portion of the model, upstream of the nozzle, was arbitrary. A sheet metal fairing was used at the wing trailing edge so that induced air flowed smoothly into the augmentor entrance.

The relative settings of the augmentor and nozzle were prescribed to give optimum static thrust augmentation. These settings were determined from the small-scale tests of reference 2 and are defined and tabulated in figure 5(b). The augmentor was mounted on a movable platform to facilitate the adjustments (in addition, it was possible to rotate the nozzle, the nozzle extension, and the nozzle inlet plenum about the axis of the inlet plenum, (fig. 4(a)).

Acoustic panels were mounted flush to the interior surfaces of the flap, the shroud, and the intake door (fig. 5(c)). The panels were designed to provide maximum noise reduction in the frequency range from 2 to 3 kilohertz. The two layer construction was incorporated to broaden the attenuation range. Ten different panels were used to make up the acoustic surface of the augmentor (four each on the flap and shroud and two on the intake door). The steady-state flow resistance of each panel was measured from samples of the panel material. For the face sheet - core combination, resistances ranged from 26 to 44 centimeter-gram-seconds Rayls at 132 centimeters per second. For the core-septum-core combination, resistances ranged from 39 to 67 centimeter-gram-seconds Rayls at 54 centimeters per second. Design details and acoustic characteristics of the panels are given in reference 3. To test in the hard-wall configuration, the panels were merely turned over so that the solid backing sheet was exposed to the flow.

Instrumentation

Far-field sound levels were measured by twenty 1.27-centimeter-diameter condenser microphones placed at various intervals on a 30.2-meter-radius circle around the augmentor-wing test apparatus (fig. 6(a)). These microphones were placed to measure the noise at angles corresponding to an aircraft flyover. The center of the microphone circle was located at the exit plane of the lobe nozzle when the augmentor was at a 20° angle relative to the wing chord plane ($\delta_F = 20^\circ$). The microphones were mounted on 0.32-centimeter-thick hardboard (fig. 6(b)) and placed at grade level at a distance from the center span of the augmentor model to the microphone of 30.5 meters. In effect, the microphones were located approximately 8° away from the exact flyover plane.

Sound levels were also measured at various azimuthal angles, or angles relative to the spanwise direction of the model, in order to obtain noise measurements at locations corresponding to various sideline locations. A single microphone was suspended from the boom of a mobile crane to prescribed locations. These locations are shown schematically in figure 7 for various augmentor deflection angles δ_F. The tables in the figures give the measurement locations in terms of the angle from the wing chord plane θ, the angle from the model span centerline γ, and the distance between locations measured parallel to the model span centerline m. All microphones were calibrated prior to a test run with a standard piston calibrator (124 (±0.2) dB, 250-Hz tone). The sound data were analyzed by a 1/3-octave-band spectrum analyzer that determined sound pressure level spectra referenced to 20 $\mu N/m^2$.

Airflow rate was measured by an orifice flowmeter located in a straight section of the underground air supply line upstream of the gate shutoff valve (fig. 3). Pressure drop across the orifice and static pressure upstream of the orifice were measured by strain-gage pressure transducers. Strain-gage pressure transducers were also used to measure nozzle inlet total pressure, nozzle feed plenum pressure, static pressures along the augmentor inner surfaces (in the chordwise direction at center span), and total pressures at the augmentor exit plane. Nozzle inlet total pressures were measured at 11 spanwise locations inside the nozzle extension (fig. 4(a)). Total pressures at the augmentor exit were measured with a rake assembly that could be moved to any spanwise position. The rake was removed when sound data were recorded. Total pressures downstream of the nozzle exit, with the augmentor removed, were measured with a total pressure rake and a traversing total pressure probe.

Temperatures were measured by thermocouples placed upstream of the flow-measuring orifice and inside the nozzle feed plenum. All flow data were recorded and processed by the Center's central data processing system. Weather data (barometer, temperature, humidity, and wind speed and direction) were also recorded.

Procedure

The model was set up for a given configuration according to the dimensions given in the table in figure 5(b). Special care was taken in adjusting for the z-dimension given in the table since the amount of static thrust augmentation was most sensitive to this setting (ref. 3). For a given configuration, tests were performed for both the hard-wall case and with the acoustic panels installed. The test procedure was merely to set a nozzle total pressure by adjusting the airflow rate with the flow control valve. Nozzle pressure ratio ranged from 2.6 (typical takeoff condition) to 1.6 (typical landing condition). Pressures and temperatures were allowed to stabilize before acoustic measurements were taken.

Noise data were then taken at each microphone location in succession. After three data samples for each microphone were taken, the airflow rate was changed and the process repeated. The three samples of noise data at each microphone were averaged and corrected for atmospheric attenuation (ref. 4) to give lossless sound pressure levels at 30.5 meters for the microphones in the flyover plane. The flyover lossless sound pressure levels were then reduced by 6 decibels to correct for pressure doubling (height of the microphone was actually 1.27 cm above grade level, fig. 6(b)) to give lossless free-field sound pressure levels at 30.5 meters. From the lossless free-field sound pressure level spectra, overall sound pressure levels were calculated for each microphone location.

For the sound measurements in other azimuthal directions (fig. 7), the actual distance from the microphone to the center of the gound-level microphone circle was used to correct for atmospheric attenuation and ground reflection effects (ref. 5) in order to obtain lossless free-field sound pressure levels.

The method of extrapolation of the model data to a full-size, 91 000-kilogram aircraft is given in appendix B.

Nozzle exhaust velocities were calculated from the isentropic equations by using the total pressures and temperatures measured upstream of the nozzle exit. Free-stream jet velocities (with the augmentor removed) and velocities at the augmentor exit, again, were calculated from the isentropic equations by using total pressures measured by probes placed downstream of the nozzle exit. Static pressures were assumed to be atmospheric, and the total temperature was taken as that measured in the nozzle feed plenum.

AERODYNAMIC RESULTS

The aerodynamic results for the nozzle alone are presented in terms of velocity profiles at various axial locations downstream of the nozzle exit and peak velocity decay rate as a function of axial distance. The augmentor aerodynamic results consist of velocity profiles at the augmentor exit for various augmentor settings δ_F, jet velocities, spanwise locations, and lateral distances from the nozzle to the flap (z-dimension, fig. 5(b)). Also included is a comparison of augmentor exit velocity profiles for the large-model tests and small-model tests of reference 3. In addition, augmentor inner surface static pressures are presented.

Nozzle Alone

Velocity profiles at three different axial locations downstream of the nozzle exit, with the augmentor removed, are shown in figure 8. The profiles are shown in the spanwise direction across the nozzle array at the centerline of the individual lobes.

The data shown in figure 8(a), for $x = 27.9$ centimeters (or $x/D_{et} \approx 1.0$), were obtained from a total pressure probe that was traversed across the two outermost lobes. The flow from each individual lobe is clearly defined at this axial location. Farther downstream (fig. 8(b)) the flow has partly coalesced but still exhibits peaks from the individual lobes. Finally, at a distance of 154.9 centimeters downstream of the nozzle exit (fig. 8(c)), the flow has totally coalesced and the velocity has been reduced to about 50 percent of that measured near the nozzle exit ($x = 27.9$ cm, fig. 8(a)).

Peak velocity decay as a function of distance from the nozzle exit is shown in figure 9 for two different nozzle pressure ratios. For the 2.6-pressure-ratio data, two values are given for the nozzle exhaust velocity (velocity at $x = 0$). The higher velocity (361 m/sec) was calculated from the isentropic equations by assuming total expansion. The lower velocity (323 m/sec) was the calculated sonic velocity using the total temperature measured in the nozzle feed plenum. Based on the 1.6-nozzle-pressure ratio data, the potential core length, or the distance from the nozzle exit to the location where velocity decay starts, is about five times the equivalent diameter of an individual lobe ($D_e = 3.98$ cm). The potential core length was taken as that distance where the nozzle exhaust velocity intersected the extrapolated decay curve. Downstream of the potential core, figure 9 shows that the velocity decays quite rapidly.

With Augmentor at Setting of 20° (Takeoff)

All aerodynamic data for the augmentor are presented for the hard-wall case but are believed to be representative of the augmentor with acoustic treatment applied to the inner surfaces of the flap, the shroud, and the intake door.

Velocity profiles at the augmentor exit, at midspan, for two values of jet velocity are shown in figure 10(a). The z-dimension for this case is set for the optimum thrust condition (z = 4.44 cm). The profiles are similar in shape for either jet velocity, showing a double peak in the profile with flow attachment at the shroud (a finite velocity) and, it is assumed, flow separation at the flap (zero velocity).

Velocity profiles at approximately the 1/4- and 3/4-span locations (s = 50.16 cm and s = 140.33 cm, respectively) are compared with the midspan profile in figure 10(b). Again, the z-dimension was set for the design condition (optimum static thrust) and the jet velocity was the same for each case. It is apparent from the figure that the flow is not uniform in the spanwise direction at the augmentor exit. The flow completely fills the augmentor at a span location of 50.16 centimeters, as indicated by flow attachment at both the flap and the shroud. However, flow separation occurs at the flap for the other span locations shown.

Flow separation at or near the augmentor exit is obviously detrimental to the performance of the device. Thrust measurements were not made for the tests described herein to determine the flow separation effects. However, tests were performed with various values of the z-dimension to see if it was possible in this manner to eliminate flow separation at the augmentor exit. The results of the tests are shown in figure 10(c), where velocity profiles are given at midspan and at the same jet velocity. As the nozzle is moved closer to the leading edge of the flap (decreasing z), a higher velocity occurs at the flap trailing edge. However, flow separation occurs at the shroud surface; even the first small change (from 4.44 cm to 2.54 cm) causes flow separation. Evidently, prevention of flow separation is quite sensitive to the location of the nozzle relative to the flap for this configuration ($\delta_F = 20^\circ$). These results agree with those reported in reference 3, where it was pointed out that static thrust augmentation was a very sensitive function of z.

Velocity profiles at the 1/4- and 3/4-span locations for z of 2.54 and 0.63 centimeter were similar to those shown in figure 10(c) measured at midspan. That is, the flow appeared to be more uniform in the spanwise direction for these z-dimensions than for the design condition (z = 4.44 cm, fig. 10(b)).

The velocity profiles for the large and small scale models (ref. 3) are shown in figure 11 for an augmentor setting of 20°. The data are presented in terms of the nondimensional ratio of the distance from the flap to the total augmentor height measured at the augmentor exit as a function of local Mach number. Data at the 1/4-span location are used for the comparison. The profile at the 3/4-span location for the small scale model was similar to the 1/4-span data shown in the figure. The flow from the small model completely fills the augmentor (no separation), but the data for the large model indicate flow separation at the flap surface.

With Augmentor at Setting of 65° (Landing)

Velocity profiles for three different spanwise locations for a z-dimension of -2.97 centimeters (optimum thrust condition) are shown in figure 12(a). For this augmentor setting ($\delta_F = 65^\circ$) the flow from the lower portion of the nozzle lobes impinges upon the leading edge of the flap. The increase in flow turning as a result of an increase in Coanda efficiency eliminates flow separation from the flap. Also, with the relatively large angle between the nozzle and augmentor axes (45°), the flow from the upper portion of the nozzle lobes impinges upon the shroud inner surface and results in flow attachment at the shroud trailing edge. The profiles for the design condition shown in figure 12(a) indicate uniform flow across the augmentor in the spanwise direction.

Figure 12(b) shows a comparison of the profile at midspan for the design z-dimension (-2.97 cm, fig. 12(a)) and the profile when the z-dimension is increased to +2.97 centimeters. As shown in the figure, when the nozzle flow does not impinge on the flap leading edge (z = +2.97 cm), flow separation occurs at the flap trailing edge. At other spanwise locations, the profiles for a z-dimension of +2.97 centimeters were similar to that at midspan (fig. 12(b)).

The velocity profiles obtained from the large and small model tests (ref. 3) for an augmentor setting of 65° are compared in figure 13. The data are for the 1/4-span location but are typical of the profiles at other spanwise locations. The profiles from the two tests for this augmentor setting are in better agreement than was displayed for an augmentor setting of 20° (fig. 11).

With Augmentor at an Intermediate Setting of 40°

An augmentor setting of 40° possibly represents a configuration to be used either for an aircraft in a hold position over a landing site or for an aircraft operating from a longer runway than has been generally proposed (i.e., >610 m).

Velocity profiles at the augmentor exit for this augmentor setting are shown in figure 14. The flow for the design condition (fig. 14(a)) is shown to be uniform across the augmentor in the spanwise direction, with flow attachment at both the flap and shroud trailing edges. When the z-dimension is changed to -1.27 centimeters, the velocity profile is changed to that shown in the comparison plot of figure 14(b). That is, the velocity at the trailing edge of the flap increases and the velocity at the shroud decreases (compared with the design z-dimension).

Augmentor Static Surface Pressures

Variation of the static pressures at midspan along the augmentor is shown in figure 15. The pressures are presented in terms of the ratio of the absolute static surface pressure to the atmospheric pressure as a function of the distance from the trailing edges of the flap and shroud. The pressure ratios are given for the different configurations at optimum static thrust conditions. At a given nozzle jet velocity (figs. 15(a) to (c)), increasing the angle between the wing chord plane and augmentor axis (augmentor setting δ_F) causes the shroud pressures in the throat region of the augmentor to increase and the flap pressures to decrease. For an augmentor setting of 65° and nozzle jet velocity of 278 meters per second (fig. 15(d), design approach condition), the shroud static pressures are only slightly below atmospheric pressure, with the flap pressure in the throat region about 10 percent lower than atmospheric.

ACOUSTIC RESULTS

Augmentor sound levels are presented herein for various augmentor deflection angles and nozzle pressure ratios. Scaling laws are checked by comparing the data from two different model sizes. The performance of the acoustic panels is assessed by comparing hard-wall and soft-wall flyover noise levels. Finally, the lossless, free-field, large-model data are extrapolated to a full-size aircraft, and perceived noise levels at a 152.4-meter sideline distance are presented for both the approach and takeoff conditions. The method of scaling the model results to a full-size aircraft with zero angle of attack is given in appendix B. The acoustic results for the corrugated-lobe nozzle alone are presented in appendix C.

Augmentor at Approach Conditions

To simulate the approach condition, the angle between the augmentor axis and the wing chord plane δ_F was set at 65°. This section presents the acoustic data for this configuration. A nozzle pressure ratio of 1.6 would be used for the approach condition, but the data are presented over a range of pressure ratios to demonstrate the variation of the sound data with this parameter.

Comparison of large-model and scaled-up small-model data. - The data presented in reference 3 were obtained from a model augmentor wing that was one-third the size, in terms of nozzle lobe height, of the model tested and reported herein. Reference 3 presents data that are scaled to the large model for both the 65° and 20° augmentor settings without acoustic treatment (hard wall). In scaling the data the differences in nozzle height, span, and temperature and in microphone distances from the model were taken into account.

The lossless, free-field, 1/3-octave-band sound pressure level spectra for an augmentor setting of 65° are compared in figure 16 for the two models. The data are for a directivity angle of 65°, or near the location where the peak flyover noise occurs (next section). Agreement between the two sets of data is considered to be very good and substantiates the validity of the scaling laws for the two geometrically similar models for this augmentor setting.

Comparison of flyover data with and without acoustic treatment (large model). - The performance of the acoustic panels for an augmentor setting of 65° is assessed in figures 17 to 19. Reduction in overall sound pressure level in the flyover plane as a result of the installation of the panels is shown in figure 17(a). The sound levels are reduced at all directivity angles and for both nozzle pressure ratios when the panels are installed (an exception occurs for a pressure ratio of 2.0 and an angle of 100°). The greatest attenuation occurs from 40° to 50° from the augmentor exhaust axis, corresponding to directivity angles below the wing from 65° to 75°, which is near the peak noise location.

The spectra at two locations below the wing are compared in figures 17(b) and (c). The spectra at 75° (fig. 17(b)) represents the spectra at the peak flyover noise location. A reduction in sound levels above 400 hertz occurs when the panels are installed, with the greatest reduction in the frequency range 1000 to 4000 hertz. At a directivity angle of 95° (fig. 17(c)), similar trends are noted but the sound levels are attenuated less than that at 75°.

Variation of overall sound pressure level with jet velocity at various directivity angles below the wing is shown in figure 18. The jet velocity is the ideal, fully expanded velocity based on the nozzle total pressures and temperatures. For the angles shown, the attenuation is almost constant for all jet velocities. Also, as illustrated earlier in figure 17(a), as the directivity angle increases the attenuation decreases. The sound levels vary as the 8th to the 10th power of jet velocity for this configuration and the directivity angles given.

In figure 19, the reduction in overall sound pressure level that occurs as a result of using the acoustic panels is given as a function of directivity angle and nozzle pressure ratio (or jet velocity). At angles greater than 75°, attenuation is essentially independent of pressure ratio. For angles less than 75°, the amount of attenuation is a function of nozzle pressure ratio. The absolute sound levels are, of course, greater with the higher pressure ratios.

Sideline sound levels (basic data). - The lossless, free-field, sound level spectra at various azimuthal angles and a constant polar angle are compared in figure 20. These data are for a nozzle pressure ratio of 1.6, a distance of 30.5 meters from the center of the ground-based microphone circle, and acoustic panels installed on the inner surfaces of the augmentor. The data were corrected for atmospheric losses and ground reflections. The data at 90° (solid symbols) are the same as those denoted by the open circular symbols in figure 17(c). An increase in the high-frequency (>2000 Hz) sound levels occurs as the wing-tip sideline direction (decreasing azimuthal angle) is approached.

Lossless, free-field, sound pressure level spectra at constant azimuthal angles and various sideline positions are shown in figure 21. The data for the sideline position of most interest are given in figure 21(a) for an azimuthal plane angle of 27°. These data when extrapolated to a distance of 170.4 meters give the spectral data needed to calculate perceived noise levels at the conventional 152.4-meter sideline location with an altitude of 76.2 meters. The sound levels and spectral shapes given in figure 21(a) are about the same over the range of distances investigated (distances between microphone locations are given in fig. 7(c)). Peak sound levels for all positions occur between 10 and 20 kilohertz, with a slight divergence in the levels in this frequency range.

At an azimuthal angle of 45° (fig. 21(b)), the peak noise level occurs at about 8 kilohertz. The data for this angle show that sound level varies with distance from 2 to 4 decibels over the frequency range 200 hertz to 20 kilohertz. At 60° (fig. 21(c)), a rather flat peak occurs from 2000 to 8000 hertz.

In figure 22 the variation of overall sound pressure level with nozzle jet velocity is shown for two sideline locations at an azimuthal angle of 27°. A 7th-power relation exists between the sound level and the velocity. This experimental determination of the velocity dependence becomes important when scaling the data to a full-size aircraft using hot gases. This is discussed in appendix B.

Sideline perceived noise levels for a full-size aircraft. - The lossless, free-field sideline data of figure 21(a) were used to calculate perceived noise levels for a full-size aircraft. The data were extrapolated to a distance of 152.4 meters from the flyover path for a standard day of 288 K and 70-percent relative humidity. The results are given in figure 23, where perceived noise level is plotted as a function of jet velocity and/or nozzle pressure ratio. For a typical landing nozzle pressure ratio of 1.6 the calculated perceived noise level at both sideline positions given in the figure is of the order of 98 PNdB. Note that the data in figure 23 are for zero angle of attack (wing chord plane parallel to the ground plane). With a nonzero angle of attack the measuring points would have to be shifted forward (toward the direction of flight) and the data corrected for the change in acoustic path length.

Augmentor at Takeoff Conditions

The data for a typical takeoff configuration are characterized by an augmentor setting δ_F of 20° and a design nozzle pressure ratio of 2.6. The data again are presented over a range of nozzle pressure ratios (or jet velocities) to show the acoustic data variation with this parameter.

Comparison of large-model and scaled-up small-model data. - One-third octave band spectra for the two model sizes are shown in figure 24. Both sets of data are for the hard-wall augmentor configuration and are lossless, free-field data at a directivity angle of 110° and a distance of 30.5 meters. Above 800 hertz the data begin to diverge considerably, with the scaled-up, small-model data having higher values of sound pressure level. For an augmentor setting of 20° then, it is obvious that the scaling laws do not work for these two different models. The lack of agreement in the acoustic data might imply that the two models were operated at different configuration settings and therefore were not geometrically similar. This is partially substantiated by the lack of agreement between the augmentor exit velocity profiles shown in figure 11. However, results from acoustic tests where the geometrical parameters (z, l_z, and augmentor throat area) were varied showed minor or negligible differences from the results in figure 24. The reason for the failure of the scaling laws for this augmentor setting is unexplained at the present time.

Encouragingly, however, the results from the large scale model indicate a considerable decrease in noise levels from those predicted from the small-scale tests. Based on the data in figure 24, perceived noise levels for the large scale model would be about 7 PNdB below those calculated from the data taken in the small-model tests.

Comparison of flyover data with and without acoustic treatment. - Lossless, free-field sound levels are compared in figure 25 for the hard-wall augmentor and the augmentor with acoustic treatment applied to its inner surfaces. The overall sound pressure level directivity patterns (fig. 25(a)) suggest that the only location below the wing where the acoustic panels are effective is near the location where the hard-wall peak sound level occurs (120°). For a nozzle pressure of 2.6, the sound level at a directivity angle of 120° is reduced by about 4 decibels with a 1- or 2-decibel reduction at adjacent angles of 110° and 130°. At other angles below the wing the separation in sound levels for the two configurations is within the accuracy of the measurement.

The sound pressure level spectra at 70° (fig. 25(b)) suggest that the two sets of data (hard-wall and with acoustic treatment) are essentially invariant across the entire frequency range for either nozzle pressure ratio shown. Spectral data at the peak overall sound pressure level location of 120° are shown in figure 25(c). The reduction in sound levels at this location (120°) occurs primarily in the frequency range 800 to 6300 hertz.

Variation in overall sound pressure level with nozzle jet velocity, or nozzle pressure ratio, is shown in figure 26 for both the hard-wall and acoustic panel configurations at four different directivity angles. The sound levels vary approximately as the 5th and 6th power of the jet velocity. Slight perturbations in the data occur between velocities of approximately 300 and 320 meters per second (subsonic and supersonic jet velocities, respectively).

Sideline sound levels (basic data). - With an augmentor setting of 20° the sound levels decreased as the wing-tip sideline direction was approached. This is illustrated in figure 27, where spectral data are given for various azimuthal angles and a constant angle (90°) from the wing chord plane. These data are for the acoustically treated augmentor. The shapes of the spectra are generally the same, but the sound levels decrease as the azimuthal angle decreases. Spectra at constant azimuthal angles and various sideline locations are shown in figure 28. There appears to be a general trend toward increasing sound levels farther aft of the 90° polar plane for frequencies below 2 kilohertz. Above 4 kilohertz this trend is reversed. The variation of overall sound pressure level at positions 1 and 5 of figure 28(a) with nozzle jet velocity is shown in figure 29. A 5th power relation exists at these locations for this configuration.

The spectra for both operating conditions (takeoff and approach) at about the same sideline location are compared in figure 30. The sound levels for either configuration are about the same in the frequency 1000 to 5000 hertz, where weighting factors for perceived noise level calculations are dominant. Perceived noise levels, therefore, for either the takeoff or approach operating mode would be approximately the same.

Sideline perceived noise levels for a full-size aircraft. - The large- and small-model results shown in figure 24 must be reconciled before reliable perceived noise levels can be calculated for a full-size aircraft in the takeoff mode. In spite of the model disagreement, however, sideline perceived noise levels were calculated for a 91 000-kilogram aircraft from the large-model data shown in figure 28(a). The results of the calculation are shown in figure 31, where perceived noise level is presented as a function of nozzle jet velocity (or nozzle pressure ratio). The data are for a sideline distance of 152.4 meters on a standard day of 15° C and 70-percent relative humidity. At the takeoff nozzle pressure ratio of 2.6 the wing-tip sideline perceived noise level is approximately 97 PNdB, with a slightly lower noise level behind the aircraft.

With Augmentor at an Intermediate Setting

An intermediate augmentor setting of 40° possibly represents a configuration to be used either for an aircraft in a holding position over a landing site or for an aircraft operating from a longer runway than has been generally proposed (i.e., >610 m).

Comparison of flyover data with and without acoustic treatment. - For this augmentor setting ($\delta_F = 40^{\circ}$) the amount of attenuation realized as a result of using the acoustic panels is between that obtained for the landing and takeoff configurations. The results shown in figure 32(a) show that less attenuation is obtained than for the landing configuration (fig. 17(a)) and more than for the takeoff configuration (fig. 25(a)). Again, as with the landing and takeoff configurations, the peak overall sound pressure level below the wing occurs at 40° from the augmentor axis (directivity angle, or angle from wing chord plane, of 100°).

The spectra at two positions below the wing (figs. 32(b) and (c)) show that the sound levels above 800 hertz are most affected (attenuated) by application of the acoustic panels.

The variation of overall sound pressure level with nozzle jet velocity at several directivity angles below the wing is shown in figure 33. Attenuation occurs at all velocities and angles as a result of the application of the acoustic panels. The velocity dependence of the overall sound pressure level for the data with the acoustic panels varies between the 4th and 7th powers.

Sideline sound levels (basic data). - Representative sound levels at the sideline locations are shown in figure 34. At a constant angle from the wing chord plane and at various azimuthal angles (fig. 34(a)), the results were similar to those found for the 20° augmentor setting (fig. 28); that is, as the wing tip sideline direction is approached, the sound levels decrease.

At a constant azimuthal angle and various sideline positions (fig. 34(b)), the results show that low-frequency sound levels are dominant aft of the model (position 1) and that high-frequency sound levels are greater toward the front of the model (position 6). These trends were also similar to those found for the 20° augmentor setting (fig. 28). Variation in overall sound pressure level with nozzle jet velocity at two of the locations shown in figure 34(b) is given in figure 35. The overall sound levels for the two locations are approximately the same over the range of velocities tested, but the curves faired through the data have slightly different slopes.

Sideline perceived noise levels for a full-size aircraft. - The spectral data shown in figure 34(b) for microphone positions 1 and 6 were scaled to a 91 000-kilogram aircraft. Perceived noise levels at a sideline distance of 152.4 meters for a standard day (15° C, 70-percent relative humidity) were calculated, and the results are given in figure 36. Perceived noise levels for this configuration ($\delta_F = 40^\circ$) are somewhat intermediate between those for augmentor settings of 65° (fig. 23) and 20° (fig. 31). Very little difference in noise levels exists for the two locations given in the figure.

SUMMARY OF RESULTS

The acoustic characteristics of a uniquely designed large-scale augmentor wing model were investigated. The results can be summarized as follows:

1. Comparison of hard-wall scaled-up acoustic data from a 1/3-scale model with data from the model used herein indicated

a. That the results were in good agreement when the models were in an approach configuration, that is, an augmentor setting of 65° and a nozzle pressure ratio of 1.6

b. That the two sets of data did not agree for the takeoff configuration (augmentor at 20° and nozzle pressure ratio of 2.6). The large scale model gave spectral sound pressure levels as much as 13 decibels less than that predicted from the small-scale data. The disagreement is possibly a result of the lack of similarity in the flow field at the augmentor exit for the two models.

2. Acoustic panels reduced the sound levels from those for the hard-wall case. The panels were more effective with an augmentor setting of 65° in that greater attenuation was achieved over a larger portion of the sound field below the wing.

3. For either the approach or takeoff condition, a 97- to 98-PNdB perceived noise level at a 152.4-meter sideline distance was calculated for a 91 000-kilogram aircraft.

Lewis Research Center,
National Aeronautics and Space Administration,
Cleveland, Ohio, November 11, 1976,
505-05.

APPENDIX A

SYMBOLS

A_N	nozzle exhaust area, m^2
A_3	augmentor throat area, m^2
D_e	equivalent diameter of individual lobe, cm
D_{et}	total equivalent diameter of nozzle $\sqrt{\frac{4}{\pi} \times \text{total area}}$, cm
L_3	augmentor throat height, cm
l_z	axial distance from nozzle exit to flap (fig. 5(b)), cm
m	distance between microphones used for sideline noise measurements (fig. 7), m
PNL	perceived noise level, PNdB
s	distance in spanwise direction, cm
V_j	nozzle jet velocity, m/sec
x	axial distance from nozzle exit, cm
z	lateral distance from nozzle to flap (fig. 5(b)), cm
γ	angle to sideline microphone defined in fig. 7, deg
δ_F	augmentor setting (angle between wing chord plane and augmentor axis), deg
θ	directivity angle in flyover plane defined in fig. 6, deg
θ_D	augmentor diffuser angle, deg
θ_I	intake door angle, deg
φ	azimuthal plane angle (angle from wing spanwise direction) defined in fig. 7, deg

APPENDIX B

METHOD OF EXTRAPOLATION OF MODEL DATA TO A 91 000-KILOGRAM AIRCRAFT AND CORRESPONDING PERCEIVED NOISE LEVELS

Sideline perceived noise levels for a standard day of 15° C and 70-percent relative humidity were calculated for a full-size, 91 000-kilogram aircraft in the following manner: First, the model, lossless, free-field sound pressure levels were extrapolated to the desired distances (distance from sketch of aircraft to data points in figs. 23, 31, and 36). Reduction in sound levels due to spherical spreading and atmospheric attenuation (for 15° C and 70-percent relative humidity) were accounted for. The model spectral levels were then increased in proportion to the increase in augmentor span (13.21 m for full size).[1] This requires an increase of 8.4 decibels (10 log 13.21/1.91) in model sound pressure levels as a result of area (span) increase. Model augmentor and nozzle heights were the same as those to be used for a full-size aircraft; therefore, no correction is needed for frequency shift.

Secondly, the increase in jet temperature and its corresponding effect on jet velocity at the same nozzle pressure ratio was accounted for. The velocity increases as the square root of the ratio of the temperature of the hot gas to the temperature of the cold gas. The hot-gas temperature was assumed to be 422 K (ref. 2) since it is the flow from the relatively cool fan region of the bypass engine. The cold-gas temperature from the model tests was of the order of 288 K. The square root of the temperature ratio then becomes 1.21 ($\sqrt{422/288}$). The model experimental data were then examined to determine the velocity exponents from plots of overall sound pressure level as a function of nozzle jet velocity at the sideline location. For an augmentor setting of 65° the exponent was 7 (fig. 22), for 20° the exponent was 5 (fig. 29), and for 40° the exponents were 4 and 3.4 (fig. 35) depending on the sideline location. The increase in velocity, then, calls for a 5.8-decibel (70 log 1.21) increment to be added to the model data for a 65° augmentor setting, a 4.1-decibel increment (50 log 1.21) for 20°, and either a 3.3-decibel (40 log 1.21) or 2.8-decibel increment (34 log 1.21) for 40°. The direct dependence of sound levels on jet density has not been demonstrated and therefore was not accounted for.

After these increments in sound level were added to the model spectral data at the specified distances for a standard day of 15° C and 70-percent relative humidity, perceived noise levels were calculated by the method outlined in reference 6.

---

[1] Personal communication with J. M. Campbell, Boeing Commercial Airplane Company.

APPENDIX C

ACOUSTIC RESULTS FOR CORRUGATED-LOBE NOZZLE ALONE

Lossless, free-field acoustic data as a function of nozzle pressure ratio for the nozzle alone are shown in figure 37. The directivity patterns of overall sound pressure level (fig. 37(a)) indicate that the peak noise location is at a directivity angle of 120° from the wing chord plane (or 40° from the nozzle exhaust axis). Data were obtained with and without (not shown) the wing portion of the model installed, and the same results were obtained for both configurations.

The 1/3-octave-band sound pressure level spectra in the forward quadrant at a directivity angle of 50° (fig. 37(b)) show a small apparent effect of broadband shock noise in the high-frequency end of the spectra (>10 kHz) for a nozzle pressure ratio of 2.6 (and possibly 2.0). The spectra at the maximum overall sound pressure level location (120°, fig. 37(c)) show that the peak sound level shifts to lower frequencies as compared with those at 50° (fig. 37(b)). Also, at 120°, the shock noise, when compared with that measured in the forward quadrant, is not as severe or is masked out by the jet mixing noise. The shapes of the spectra are generally the same for all nozzle pressure ratios at a given location.

Sound pressure level spectra at other angles of interest (below the wing) and at a constant nozzle pressure ratio of 2.6 are shown in figure 38. Again, the shapes of the spectra are generally the same except for that measured at 140°, where an increase in low-frequency noise (<400 Hz) is evident. The nozzle-alone spectral data presented herein suggest that the device is primarily a source of high-frequency noise peaking from 1600 to 5000 hertz. Also, the shapes of the spectra were generally the same at all nozzle pressure ratios and all directivity angles.

Although the nozzle 1/3-octave-band spectra were free of spikes, narrowband analyses of the data (30-Hz bandwidth) indicated that screech tones were present at two microphone locations for nozzle pressure ratios from 1.8 to 2.6. The tone was most severe at a directivity angle of 50° and a nozzle pressure ratio of 2.0 (fig. 39(a)). Its peak level above the broadband noise level varied with nozzle pressure ratio and its frequency was constant at 7100 hertz for all jet velocities and locations with no evidence of harmonics. The tone was also present at a 60° directivity angle but was lower in magnitude than that at 50°. Screech tone data are summarized in figure 39(b), where the increment between the peak tone level and the broadband noise level is plotted as a function of nozzle pressure ratio for the directivity angles where the tone was detected.

Peak overall sound pressure level at 120° varied as the 8th power of the ideal fully expanded nozzle jet velocity (fig. 40). The variation at other directivity angles (not shown) ranged from the 7th power at 50° to the 8.3 power in the rear quadrant at 140°.

The acoustic characteristics of the corrugated-lobe nozzle are compared with those of other nozzle types in figure 41. The slot nozzle, with a slot length to height ratio of about 50, was fabricated and tested as a supplementary part of the program reported herein. The exit area of the slot nozzle was approximately the same as that of the corrugated-lobe nozzle (626.8 cm^2). The conical nozzle data were obtained as part of the work reported in reference 7 and are scaled from a 33-centimeter-diameter conical nozzle to the same equivalent diameter that existed for the lobe nozzle (28.24 cm). Conical nozzles would not be applicable for an augmentor-wing powered lift configuration, but the data are shown for comparative purposes. The slot nozzle, however, is directly applicable to the augmentor wing configuration.

As indicated in the figure, both the slot and conical nozzles have considerably greater noise levels in the low-frequency end of the spectra. Also, the slot nozzle is louder than the lobe nozzle at all frequencies, but the conical nozzle becomes quieter than the lobe nozzle above 6300 hertz. The peak noise level for the conical nozzle is near 1000 hertz, and that for the slot and lobe nozzles is closer to 5000 hertz.

REFERENCES

1. Dorsch, R. G.; Krejsa, E. A.; and Olsen, W. A.: Blown Flap Noise Research. AIAA Paper 71-745, June 1971.
2. Campbell, J. M.; et al.: Design Integration and Noise Studies for Jet STOL Aircraft. Task V-Noise Suppression of Improved Augmentors for Jet STOL Aircraft. (D6-60174, Boeing Company; NAS2-6344.) NASA CR-114534, 1973.
3. Jackson, John; Schedin, R. W.; and Campbell, J. M.: Design and Fabrication of an Augmentor Wing Model for Acoustic Tests. (D6-41465, Boeing Commercial Airplane Co.; NAS3-17362.) NASA CR-134518, 1973.
4. Montegani, Francis J.: Some Propulsion System Noise Data Handling Conventions and Computer Programs Used at the Lewis Research Center. NASA TM X-3013, 1974.
5. Howes, Walton L.: Ground Reflection of Jet Noise. NASA TR-35, 1959.
6. Definitions and Procedures for Computing the Perceived Noise Level of Aircraft Noise. Aerospace Recommended Practice 865A, SAE, Oct. 1964.
7. Dorsch, R. G.; Kreim, W. J.; and Olsen, W. A.: Externally-Blown-Flap Noise. AIAA Paper 72-129, Jan. 1972.

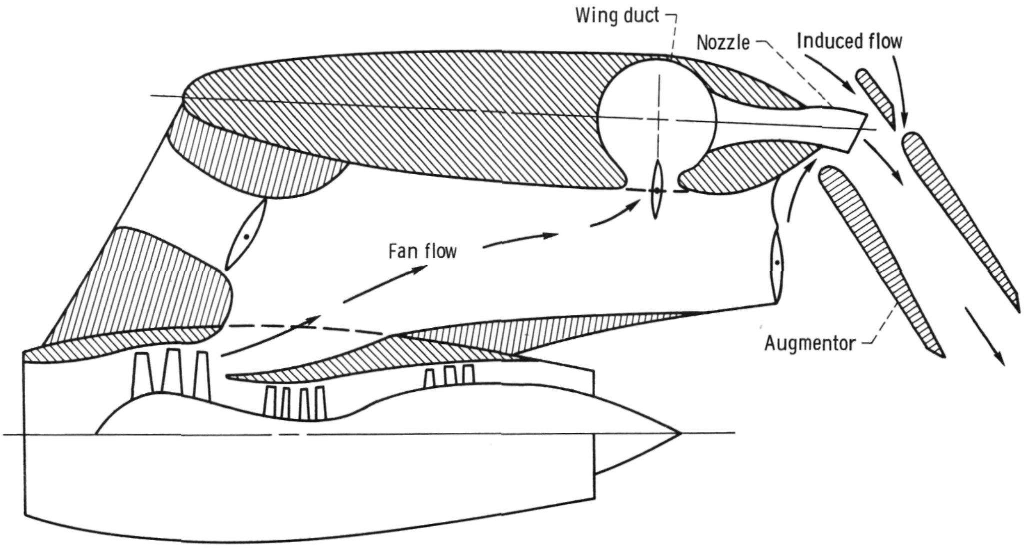

Figure 1. - Representative augmentor wing propulsion system.

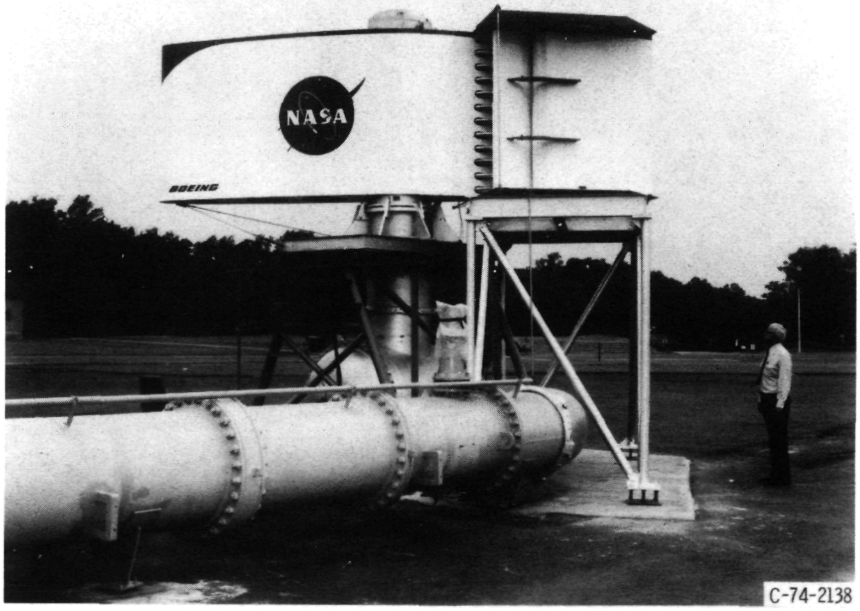

Figure 2. - Experimental facility (airflow system, nozzle, augmentor).

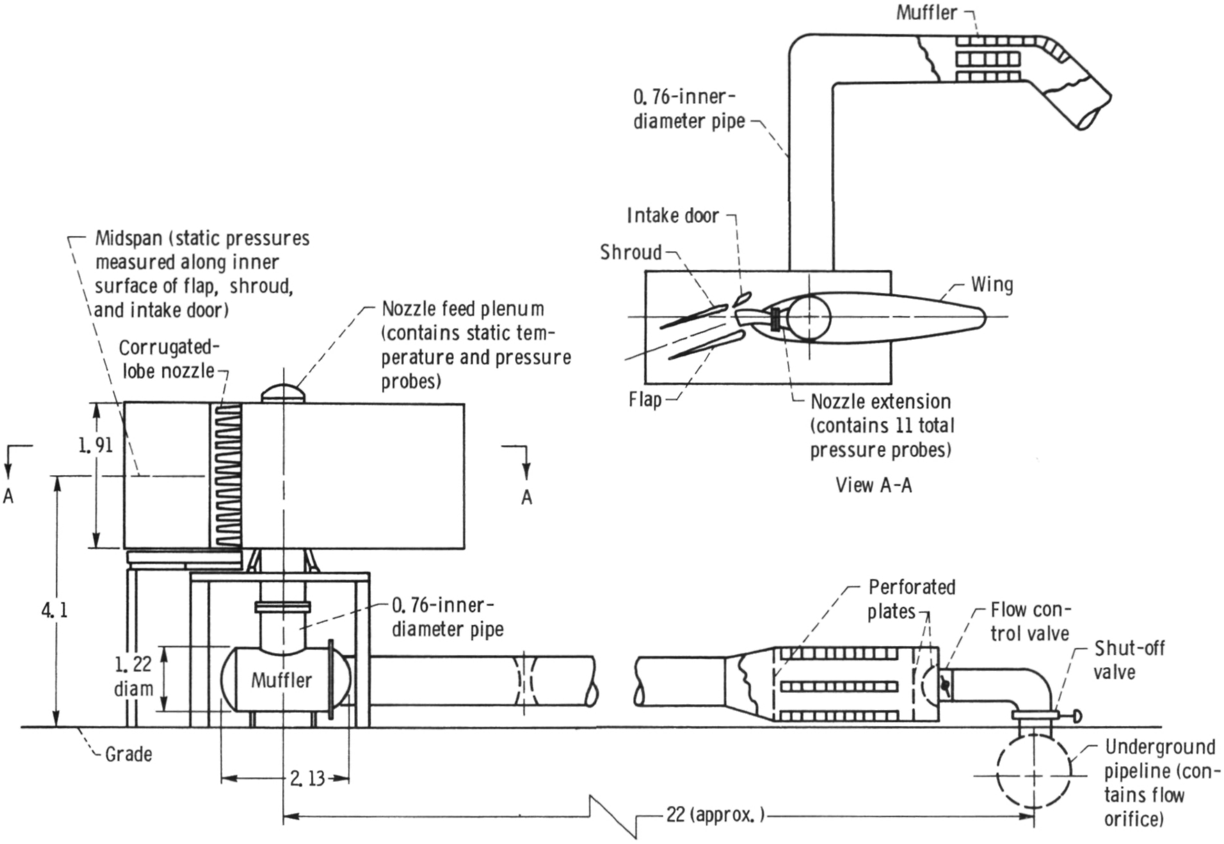

Figure 3. - Airflow system. (All dimensions in meters.)

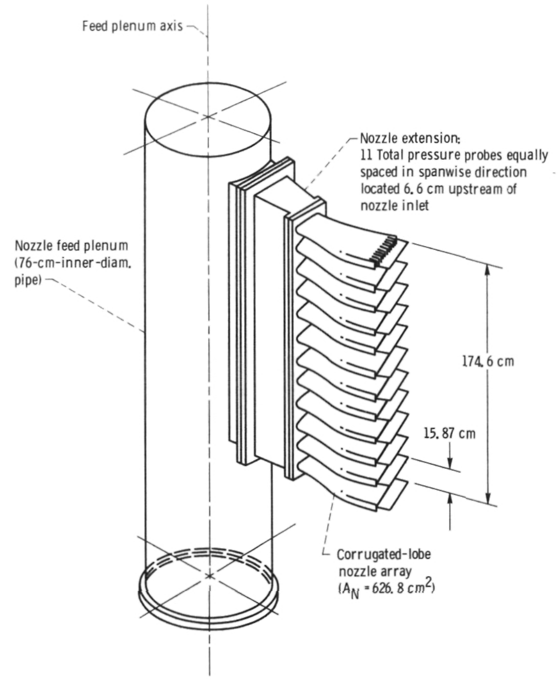

(a) General layout of corrugated-lobe nozzle, nozzle extension, and nozzle feed plenum assembly.

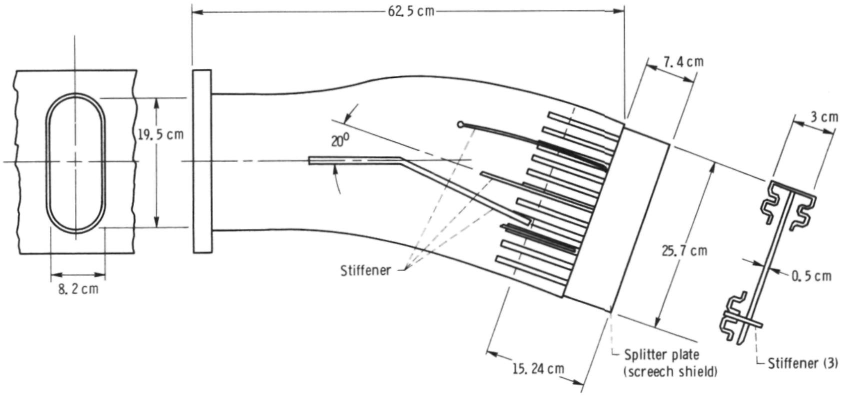

(b) Corrugated-lobe nozzle details.

Figure 4. - Corrugated-lobe nozzle configuration and dimensions.

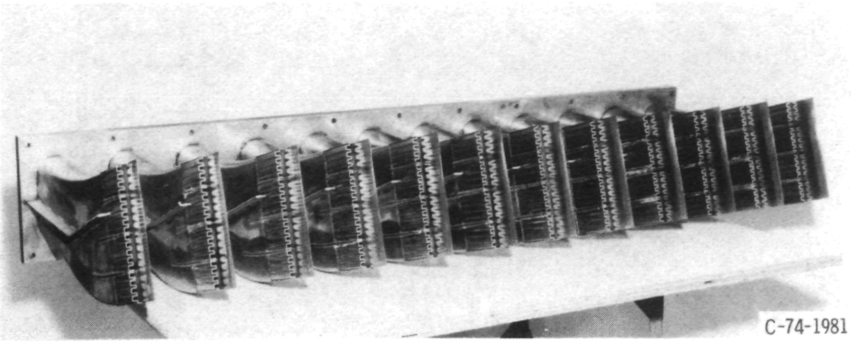
C-74-1981

(c) Complete nozzle.

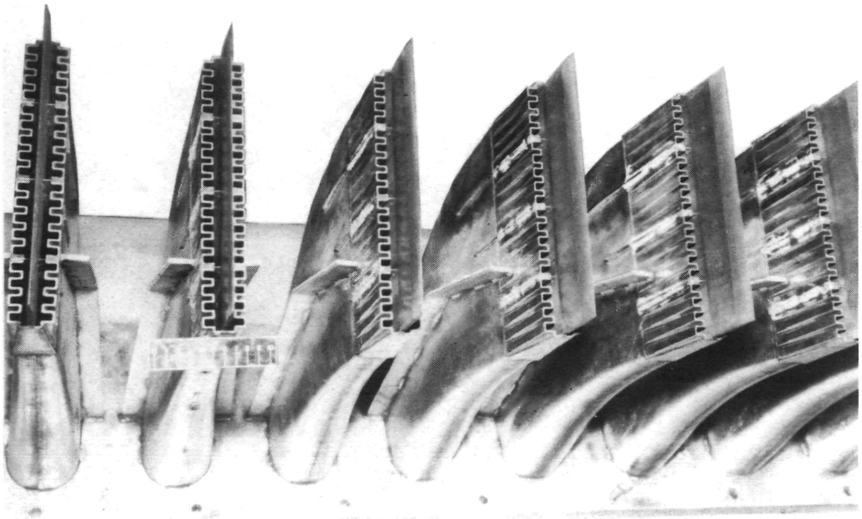
C-75-4318

(d) Closeup view of individual lobes.

Figure 4. - Concluded.

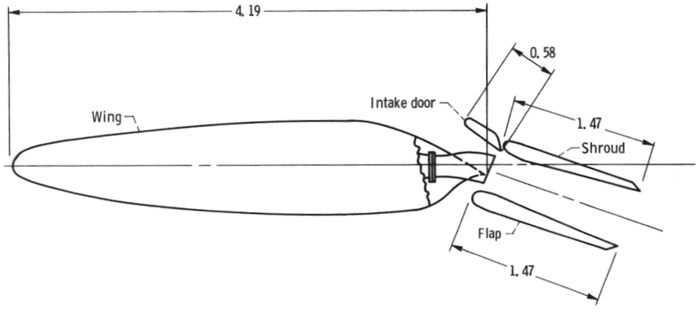

(a) General layout. Wing span, 1.91 meters. (All dimensions in meters.)

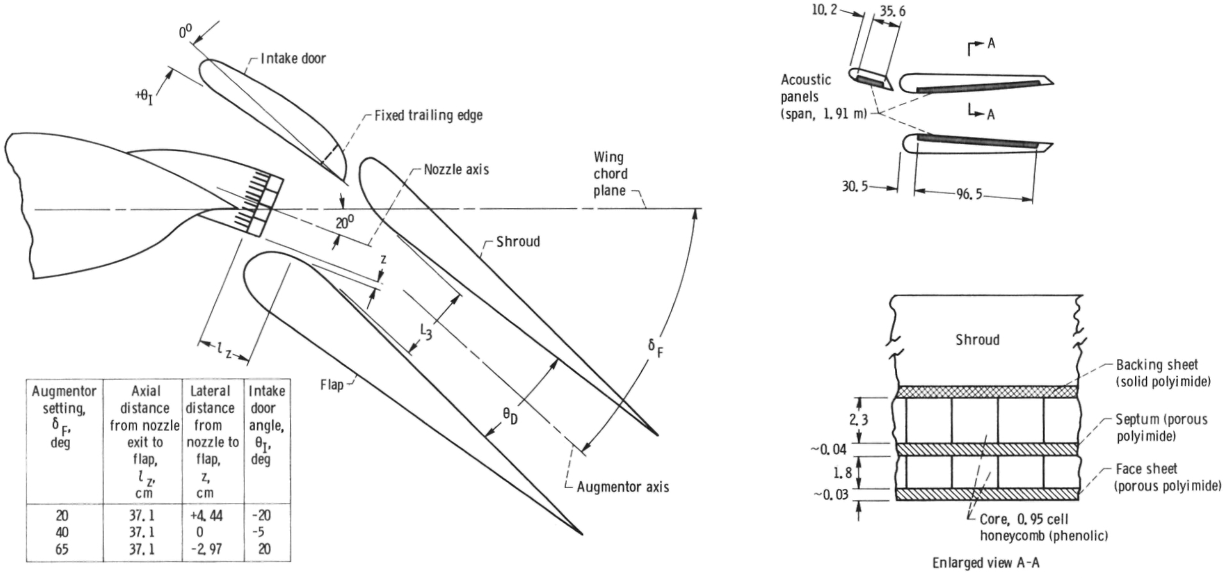

Augmentor setting, δ_F, deg	Axial distance from nozzle exit to flap, l_z, cm	Lateral distance from nozzle to flap, z, cm	Intake door angle, θ_I, deg
20	37.1	+4.44	-20
40	37.1	0	-5
65	37.1	-2.97	20

(b) Geometry for optimum thrust augmentation. Ratio of augmentor throat area to nozzle exhaust area, A_3/A_N, 11; augmentor throat height, L_3, 35.2 centimeters; augmentor diffuser angle, θ_D, 5^0. (All liner dimensions in centimeters.)

(c) Acoustic panel details. (All dimensions in centimeters.)

Figure 5. - Augmentor wing model dimensions and configuration.

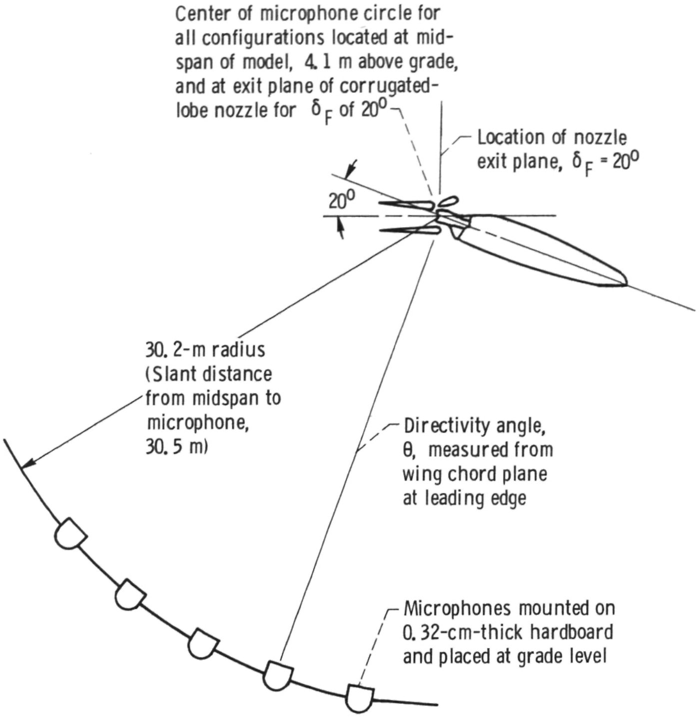

(a) Microphone layout for flyover noise measurements.

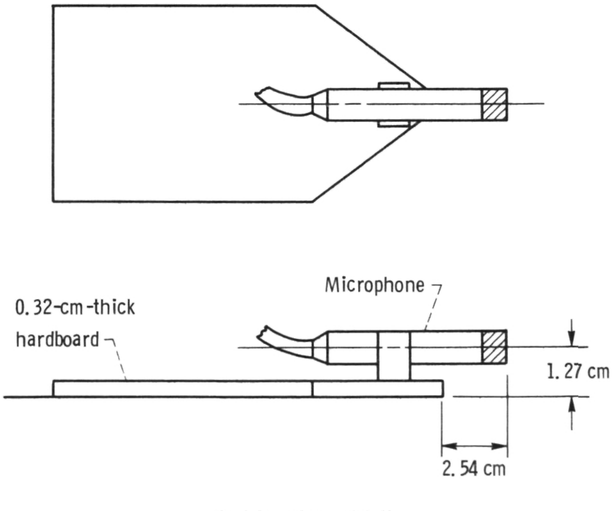

(b) Microphone detail.

Figure 6. - Acoustic instrumentation.

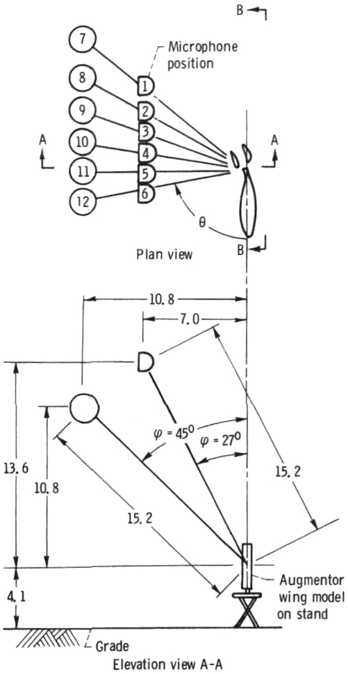

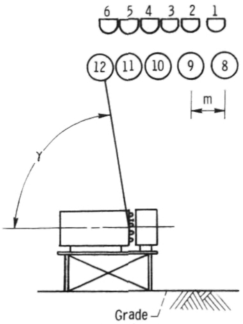

Position	Directivity angle (fig. 6), θ, deg	Angle to sideline microphone, γ, deg	Distance, m, m	
1	130	113	1-2	1.82
2	120	106	2-3	1.48
3	110	100	3-4	1.31
4	100	95	4-5	1.22
5	90	90	5-6	1.22
6	80	85	7-8	2.82
7	130	130	8-9	2.30
8	120	120	9-10	2.03
9	110	110	10-11	1.90
10	100	100	11-12	1.90
11	90	90		
12	80	80		

(a) Plan and elevation views for augmentor setting δ_F of 20°.

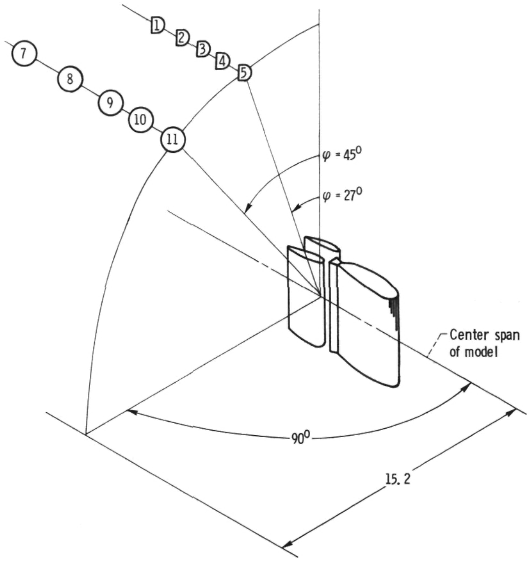

(b) Pictorial view for augmentor setting δ_F of 20°.

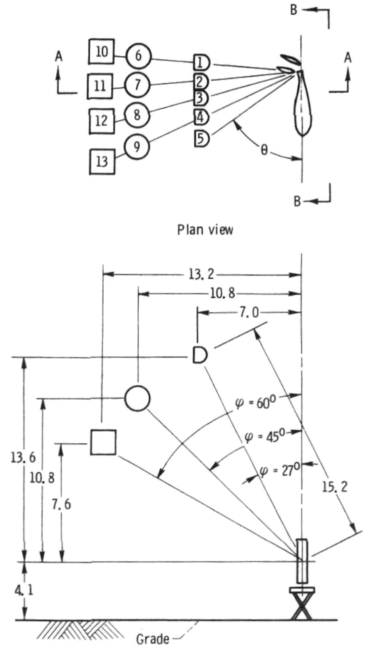

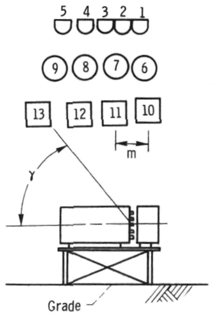

Position	Directivity angle (fig. 6), θ, deg	Angle to sideline microphone, γ, deg	Distance, m, m	
1	95	93	1-2	1.22
2	85	87	2-3	1.26
3	75	82	3-4	1.38
4	65	76	4-5	1.63
5	55	70	6-7	1.89
6	95	95	7-8	1.95
7	85	85	8-9	2.14
8	75	75	10-11	2.32
9	65	65	11-12	2.39
10	95	99	12-13	2.63
11	85	81		
12	75	65		
13	65	51		

(c) Plan and elevation views for δ_F of 65°.

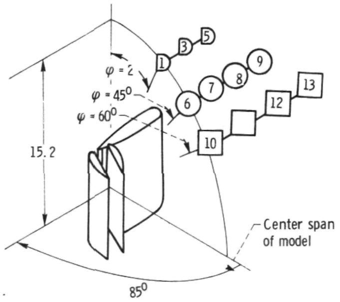

(d) Pictorial view for augmentor setting δ_F of 65°.

Fi- 7. - Microphone locations for sideline noise measurements. (All linear dimensions in meters.)

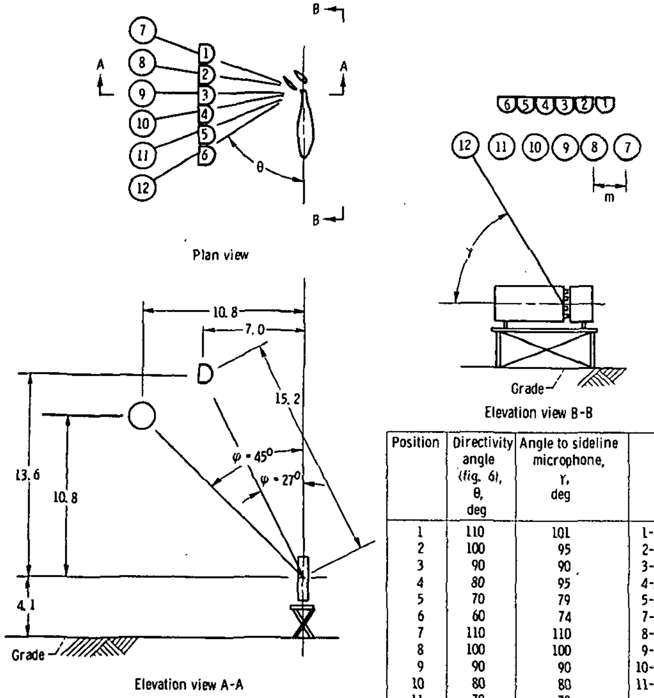

Position	Directivity angle (fig. 6), θ, deg	Angle to sideline microphone, γ, deg	Distance, m, m	
1	110	101	1-2	1.31
2	100	95	2-3	1.22
3	90	90	3-4	1.22
4	80	95	4-5	1.31
5	70	79	5-6	1.48
6	60	74	7-8	2.03
7	110	110	8-9	1.90
8	100	100	9-10	1.90
9	90	90	10-11	2.03
10	80	80	11-12	2.30
11	70	70		
12	60	60		

(e) Plan and elevation views for augmentor setting δ_F of 40°.

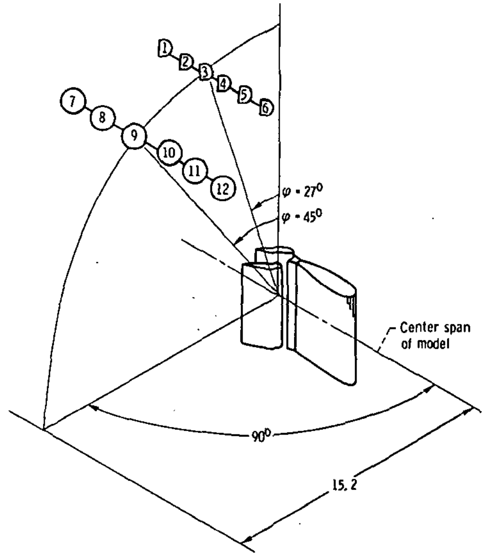

(f) Pictorial view for augmentor setting δ_F of 40°.

Figure 7. - Concluded.

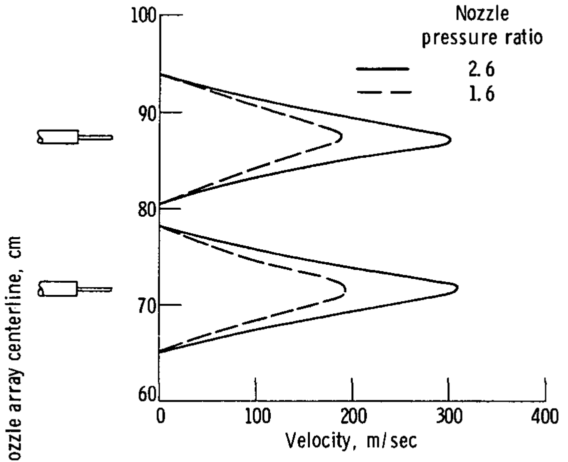

(a) Axial distance from nozzle exit, x, 27.9 centimeters.

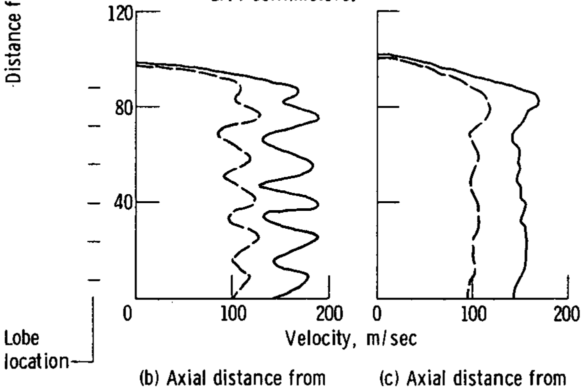

(b) Axial distance from nozzle exit, x, 86.4 centimeters.

(c) Axial distance from nozzle exit, x, 154.9 centimeters.

Figure 8. - Velocity profiles for corrugated-lobe nozzle alone (spanwise direction).

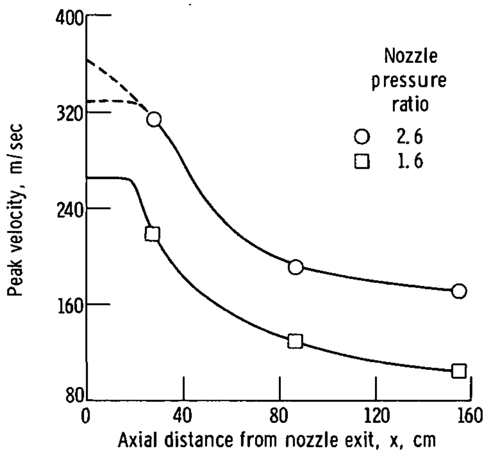

Figure 9. - Peak axial velocity decay for corrugated-lobe nozzle alone.

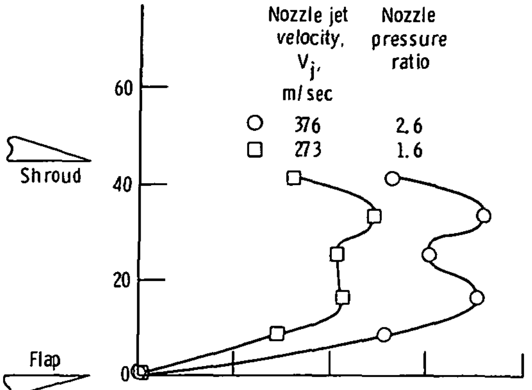

(a) Variable nozzle jet velocity; lateral distance from nozzle to flap, z, 4.44 centimeters; spanwise location, s, 95.25 centimeters (midspan).

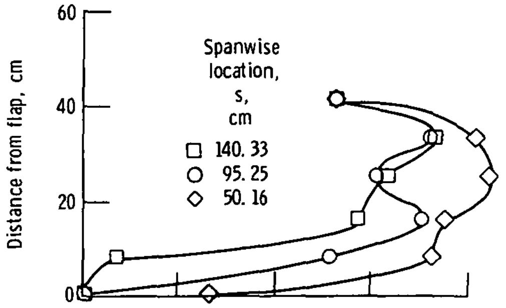

(b) Variable spanwise location; lateral distance from nozzle to flap, z, 4.44 centimeters; nozzle pressure ratio, 2.6; nozzle jet velocity, V_j, 376 meters per second.

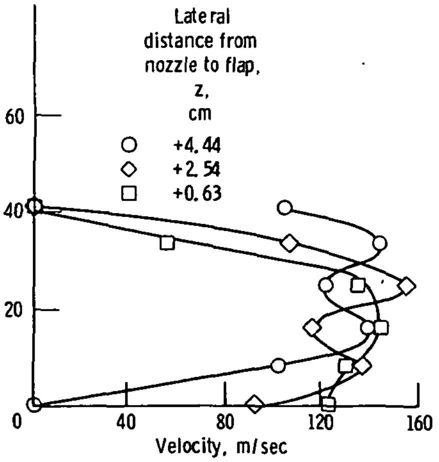

(c) Variable lateral distance from nozzle to flap; spanwise location, s = 95.25 centimeters; nozzle pressure ratio, 2.6; nozzle jet velocity, V_j, 376 meters per second.

Figure 10. - Augmentor exit velocity profiles for augmentor setting δ_F of 20°.

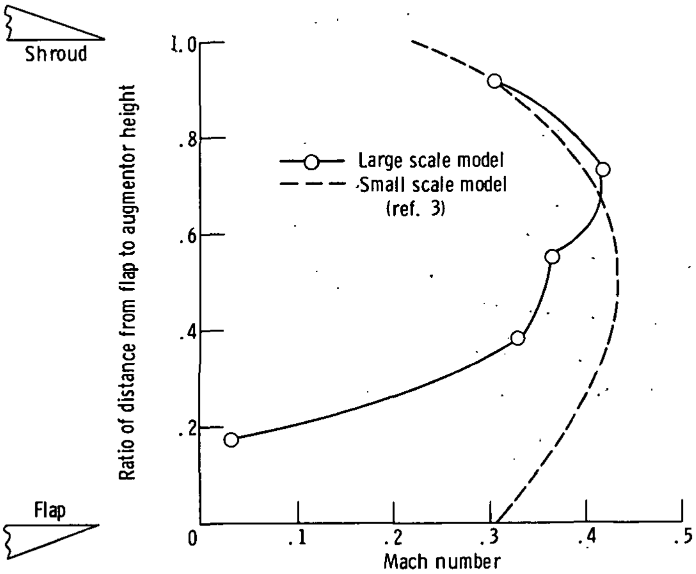

Figure 11. - Comparison of velocity profiles at augmentor exit for large- and small-scale augmentor wing models for an augmentor setting δ_F of 20°. Nozzle pressure ratio, 2.6; nozzle jet Mach number, 1.25; 1/4-span location.

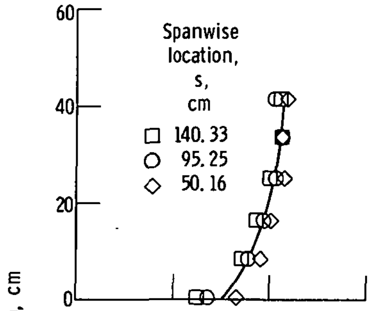

(a) Variable spanwise location; lateral distance from nozzle to flap, z, -2.97 centimeters.

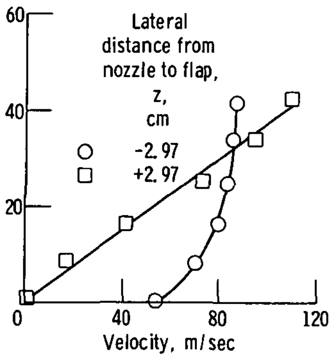

(b) Variable lateral distance from nozzle to flap; spanwise location, s, 95.25 centimeters.

Figure 12. - Augmentor exit velocity profiles for augmentor setting δ_F of 65°. Nozzle pressure ratio, 1.6; nozzle jet velocity, V_j, 269 meters per second.

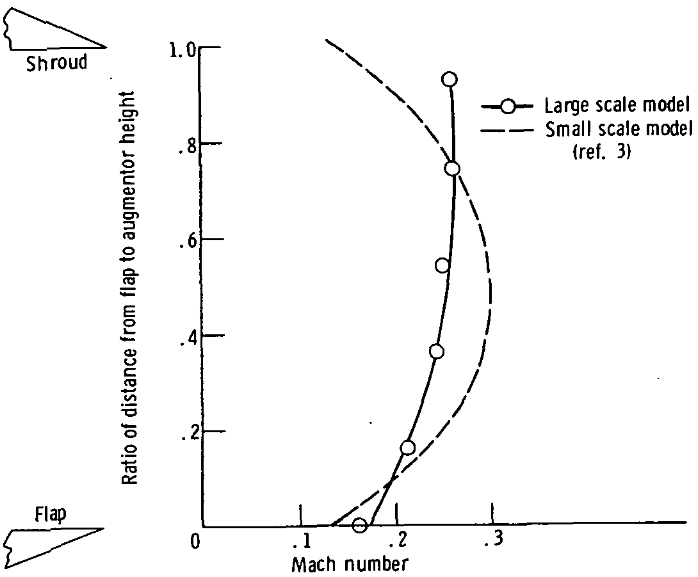

Figure 13. - Comparison of augmentor exit velocity profiles for large- and small-scale augmentor wing models for an augmentor setting δ_F of 65°. Nozzle pressure ratio, 1.6; nozzle jet Mach number, 0.85; 1/4-span location.

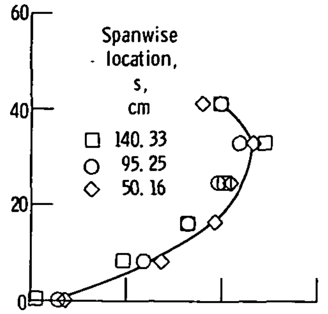

(a) Variable spanwise location; lateral distance from nozzle to flap, 0.

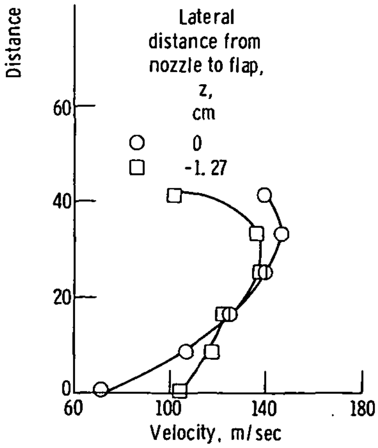

(b) Variable lateral distance from nozzle to flap; spanwise location, s, 95.25 centimeters.

Figure 14. - Augmentor exit velocity profiles for augmentor setting δ_F of 40°. Nozzle pressure ratio, 2.6; nozzle jet velocity, V_j, 371 meters per second.

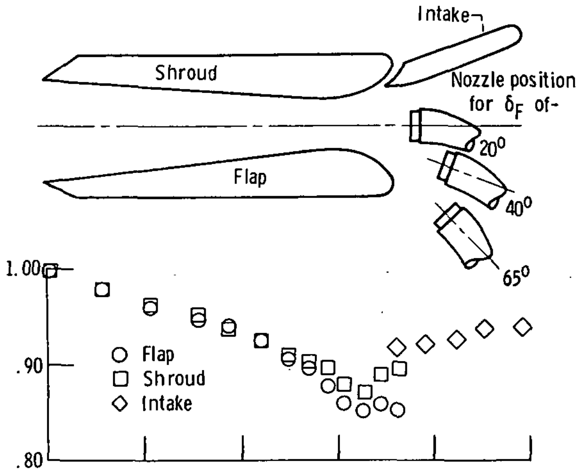

(a) Augmentor setting, δ_F, 20°; lateral distance from nozzle to flap, z, +4.44 centimeters; nozzle pressure ratio, 2.6.

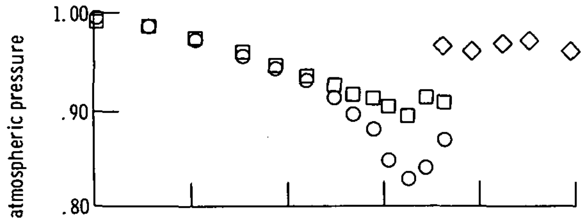

(b) Augmentor setting, δ_F, 40°; lateral distance from nozzle to flap, z, 0; nozzle pressure ratio, 2.6.

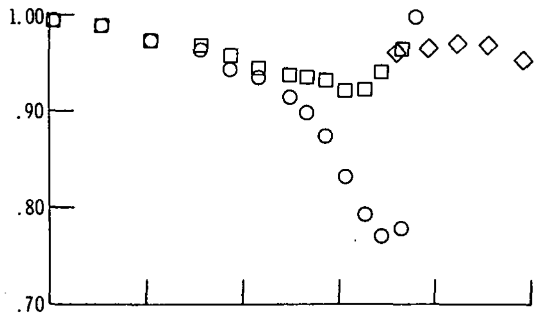

(c) Augmentor setting, δ_F, 65°; lateral distance from nozzle to flap, z, -2.97 centimeters; nozzle pressure ratio, 2.6.

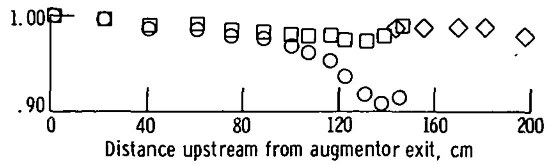

(d) Augmentor setting, δ_F, 65°; lateral distance from nozzle to flap, z, -2.97 centimeters; nozzle pressure ratio, 1.6.

Figure 15. - Static pressure profiles along inner surface of augmentor at center span. Atmospheric pressure, 99.4 kN/m^2.

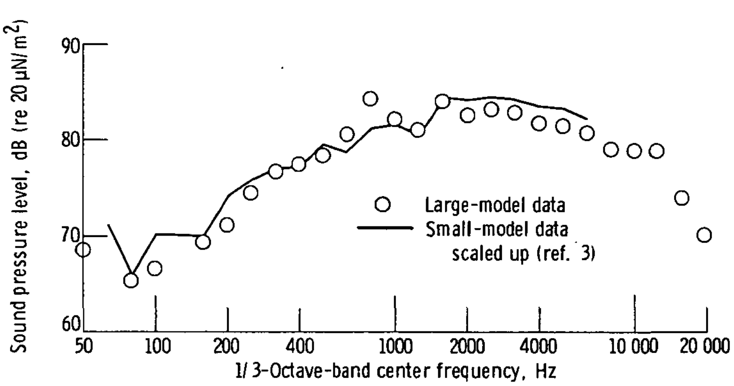

Figure 16. - Comparison of data for large and small scale models. Small-model data scaled to large-model size and operating conditions. Augmentor setting, δ_F, 65°; nozzle pressure ratio, 1.6; microphone distance, 30.5 meters; hard-wall augmentor; lossless, free-field data; directivity angle, θ, 65°.

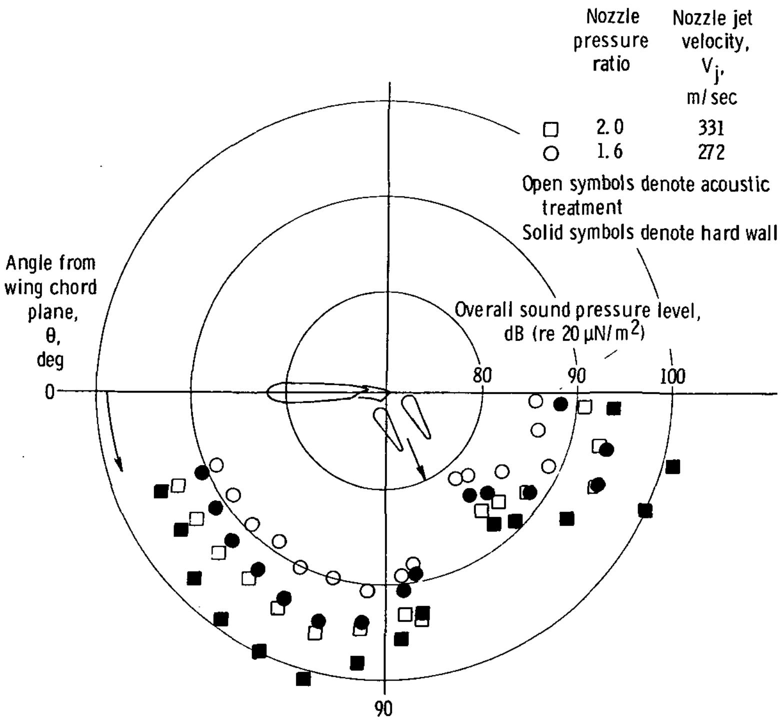

(a) Overall sound pressure level directivity patterns.

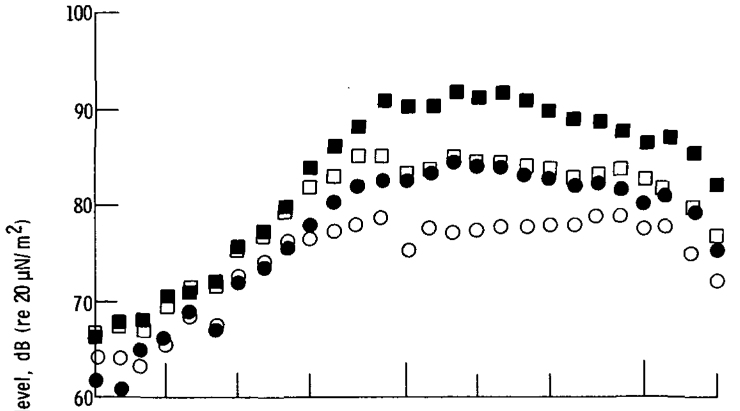

(b) 1/3-Octave-band sound pressure level at directivity angle θ of 75°.

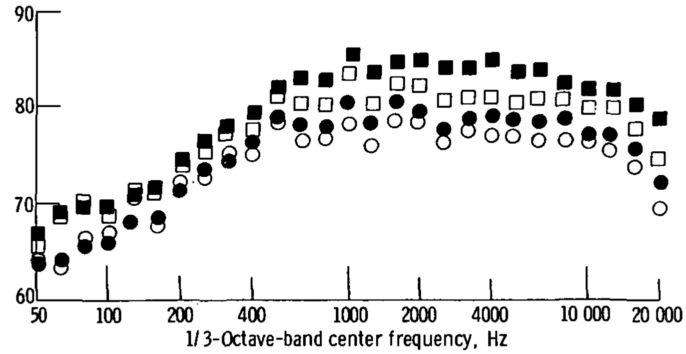

(c) 1/3-Octave-band sound pressure level at directivity angle θ of 95°.

Figure 17. - Comparison of sound levels for augmentor wing model with and without acoustic treatment. Augmentor setting, δ_F, 65°; microphone distance, 30.5 meters in flyover plane (φ = 90°).

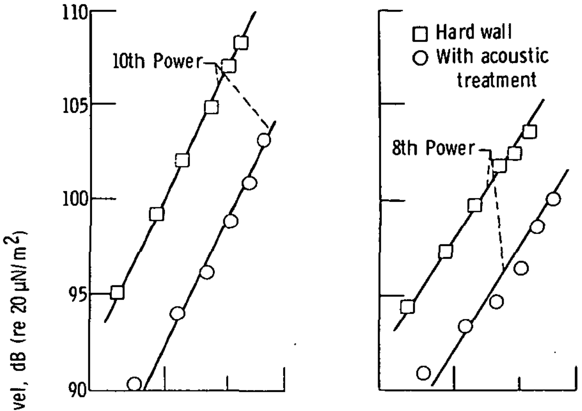

(a) Directivity angle, θ, 75°.

(b) Directivity angle, θ, 85°.

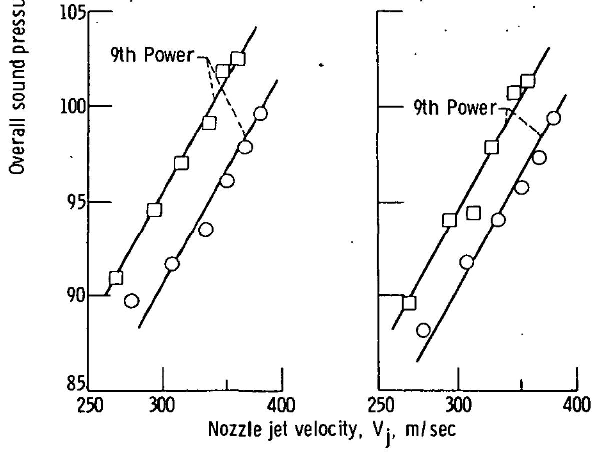

(c) Directivity angle, θ, 95°.

(d) Directivity angle, θ, 100°.

Figure 18. - Overall sound pressure level as function of nozzle jet velocity at various directivity angles. Augmentor setting, δ_F, 65°; microphone distance, 30.5 meters in flyover plane (φ = 90°).

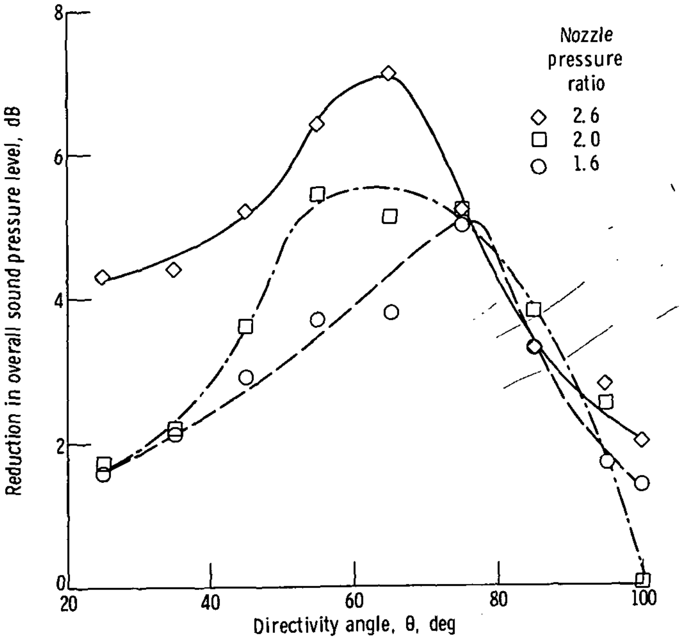

Figure 19. - Overall sound pressure level reduction in flyover plane due to acoustic treatment as function of directivity angle and nozzle pressure ratio. Augmentor setting, δ_F, 65°.

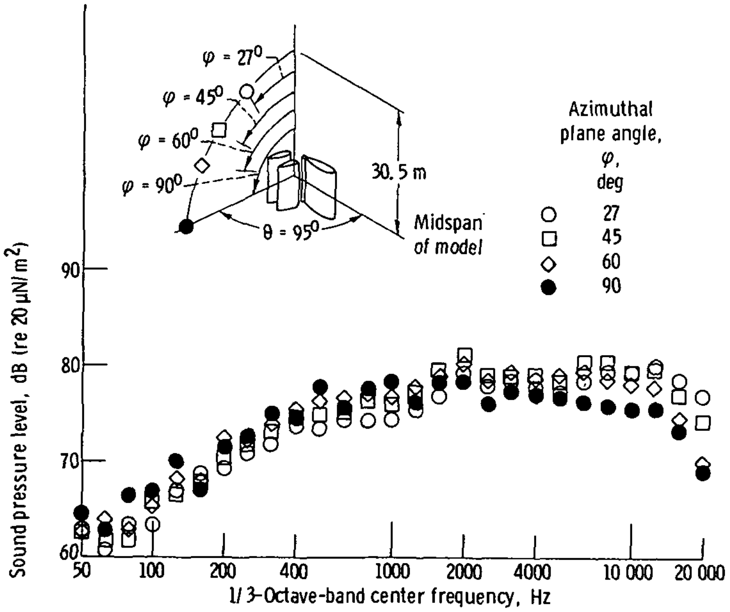

Figure 20. - 1/3-Octave-band sound pressure level spectra at various azimuthal plane angles and at a constant angle from wing chord plane (θ = 95°). Augmentor setting, δ_F, 65°; nozzle pressure ratio, 1.6; lossless, free-field data at 30.5 meters; augmentor acoustically treated.

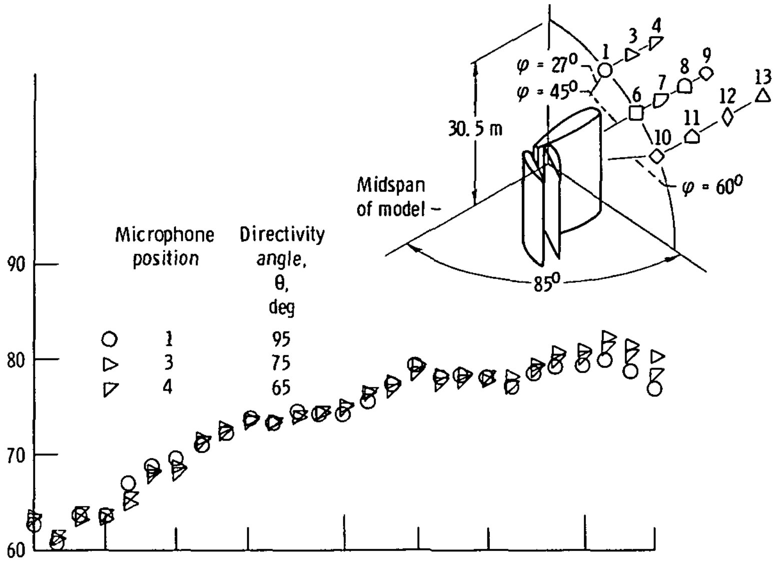

(a) Azimuthal plane angle, φ, 27°.

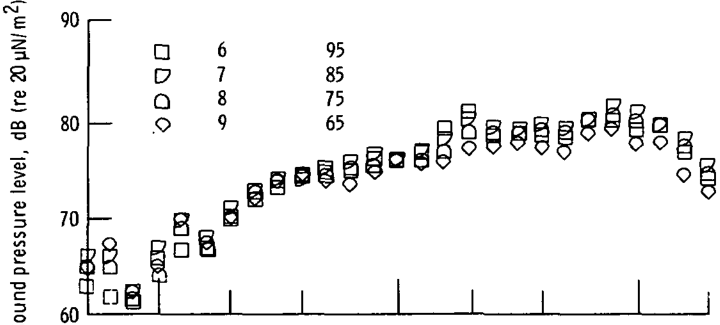

(b) Azimuthal plane angle, φ, 45°.

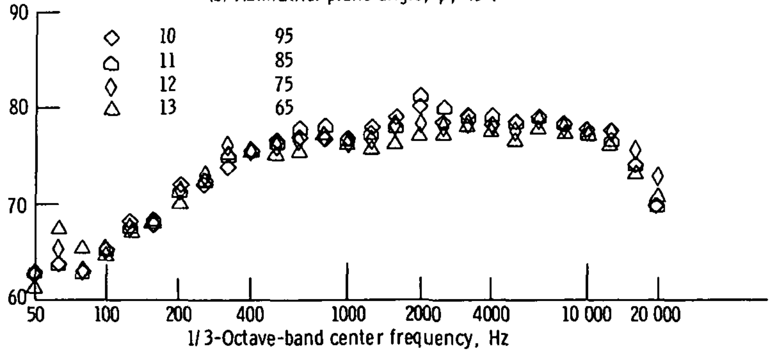

(c) Azimuthal plane angle, φ, 60°.

Figure 21. - 1/3-Octave-band sound pressure level spectra at various sideline locations. Augmentor setting, δ_F, 65°; nozzle pressure ratio, 1.6; lossless, free-field data at 30.5 meters; augmentor acoustically treated.

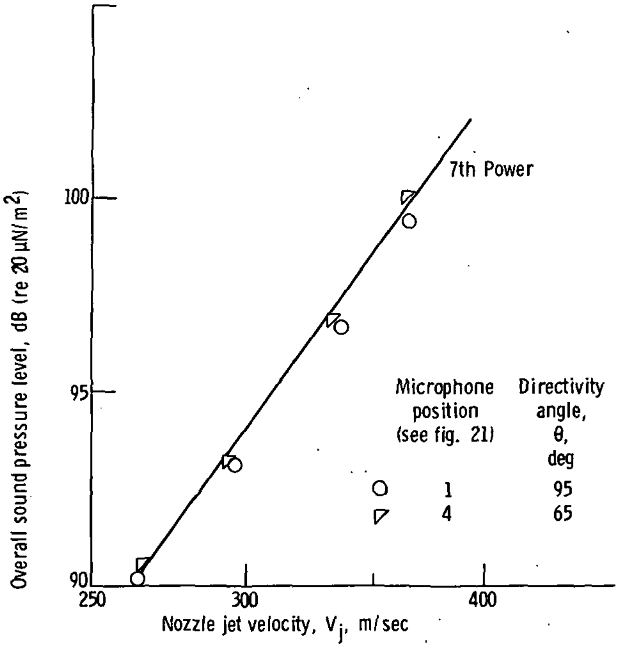

Figure 22. - Overall sound pressure level as function of nozzle jet velocity at two sideline locations for azimuthal plane angle φ of 27°. Augmentor setting, δ_F, 65°; lossless, free-field data at 30.5 meters; augmentor acoustically treated.

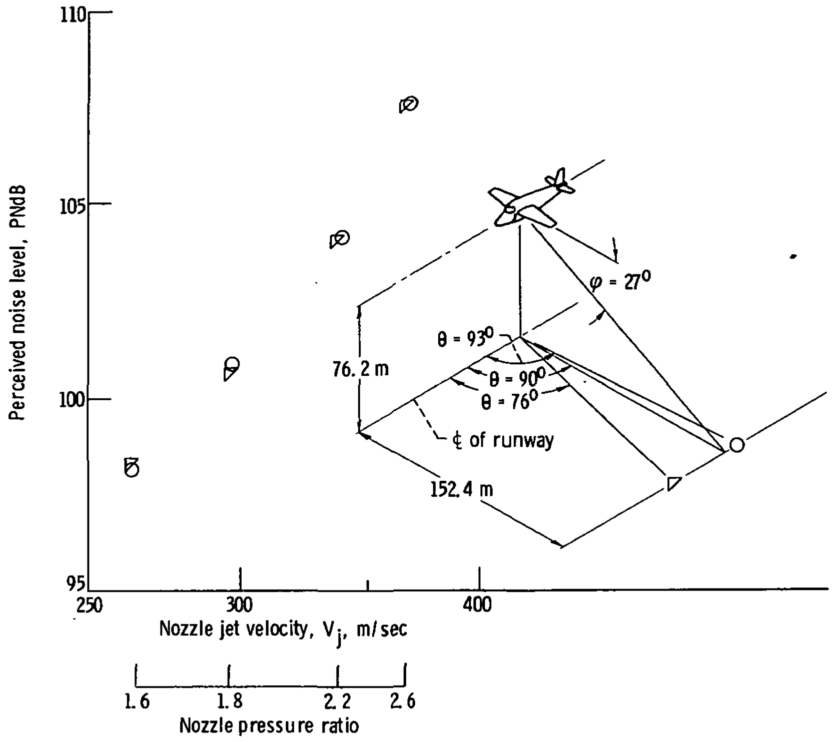

Figure 23. - Sideline perceived noise levels as function of nozzle jet velocity for 91 000-kilogram aircraft using augmentor-wing powered lift system. Augmentor setting, δ_F, 65°; augmentor acoustically treated; standard day.

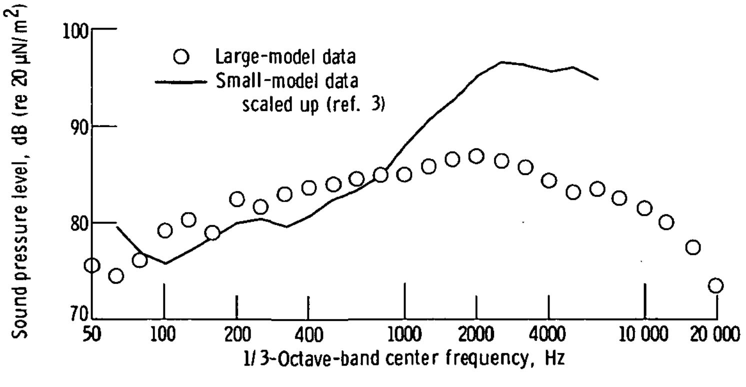

Figure 24. - Comparison of data for large and small scale models. Small-model data scaled to large-model size and operating conditions. Augmentor setting, δ_F, 20°; nozzle pressure ratio, 2.6; microphone distance, 30.5 meters; hard-wall augmentor; lossless, free-field data; directivity angle, θ, 110°.

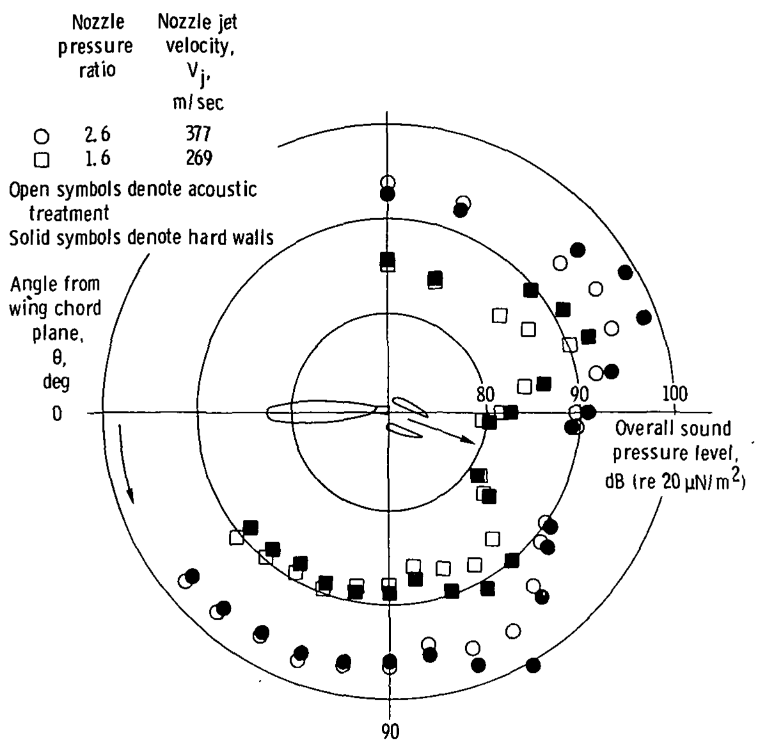

(a) Overall sound pressure level directivity patterns.

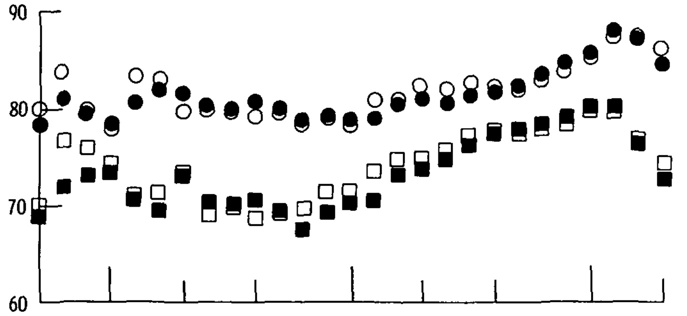

(b) 1/3-Octave-band sound pressure level spectra at directivity angle θ of 70°.

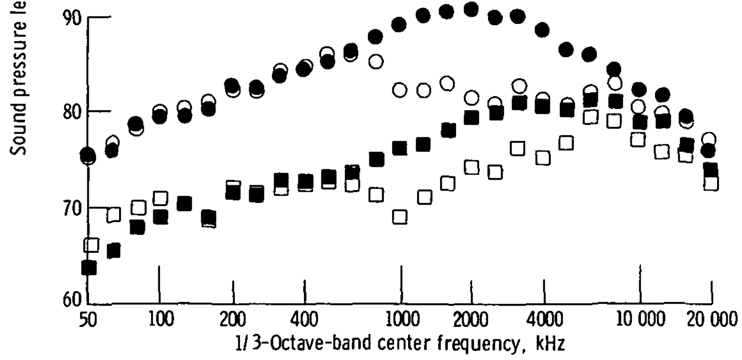

(c) 1/3-Octave-band sound pressure level spectra at directivity angle θ of 120°.

Figure 25. - Comparison of sound levels for augmentor wing model with and without acoustic treatment. Augmentor setting, δ_F, 20°; microphone distance, 30.5 meters in flyover plane (φ = 90°).

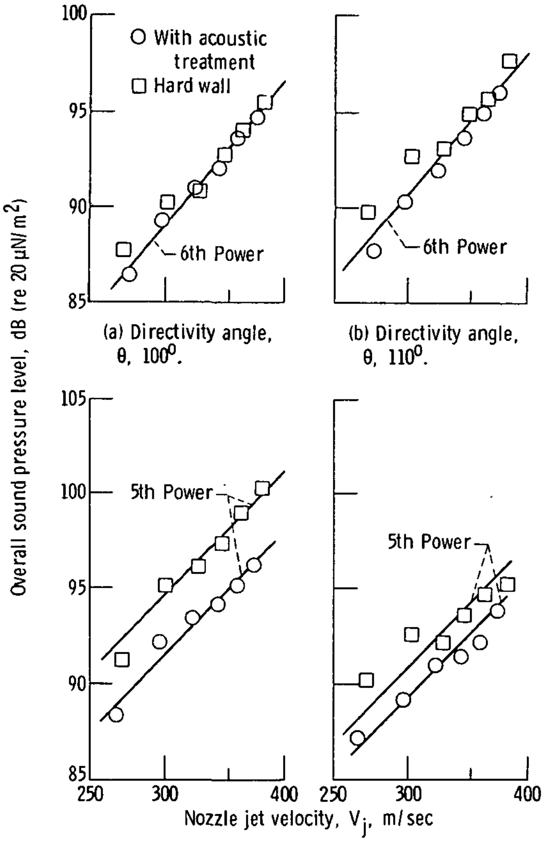

(a) Directivity angle, θ, 100°.

(b) Directivity angle, θ, 110°.

(c) Directivity angle, θ, 120°.

(d) Directivity angle, θ, 130°.

Figure 26. - Overall sound pressure level as function of nozzle jet velocity at various directivity angles. Augmentor setting, δ_F, 20°; microphone distance, 30.5 meters in flyover plane (φ = 90°).

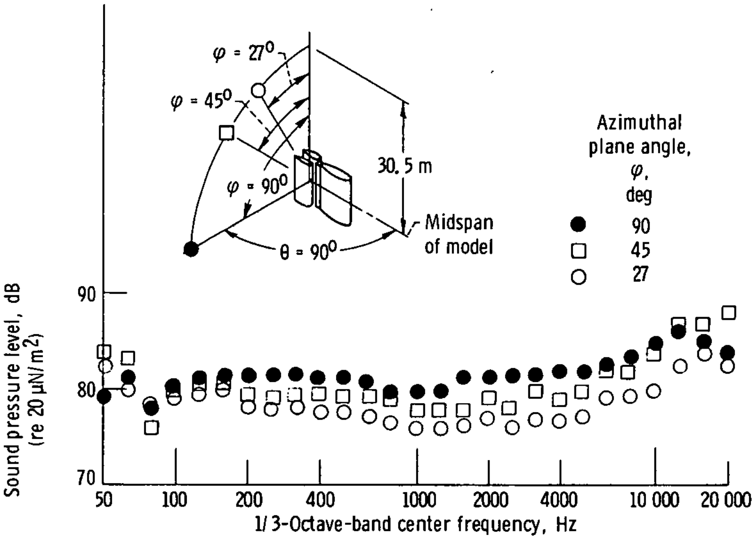

Figure 27. - 1/3-Octave-band sound pressure level spectra at various azimuthal plane angles and at a constant angle from wing chord plane (θ = 90°). Augmentor setting, δ_F, 20°; nozzle pressure ratio, 2.6; lossless, free-field data at 30.5 meters; augmentor acoustically treated.

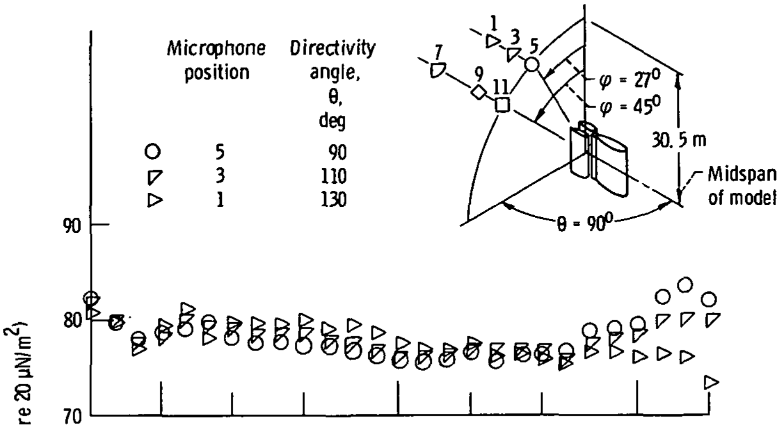

(a) Azimuthal plane angle, φ, 27°.

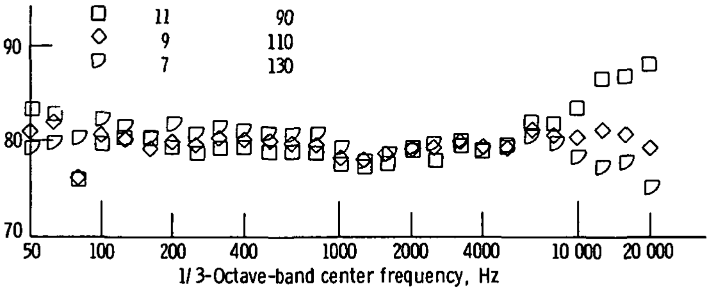

(b) Azimuthal plane angle, φ, 45°.

Figure 28. - 1/3-Octave-band sound pressure level spectra at various sideline locations. Augmentor setting, δ_F, 20°; nozzle pressure ratio, 2.6; lossless, free-field data at 30.5 meters; augmentor acoustically treated.

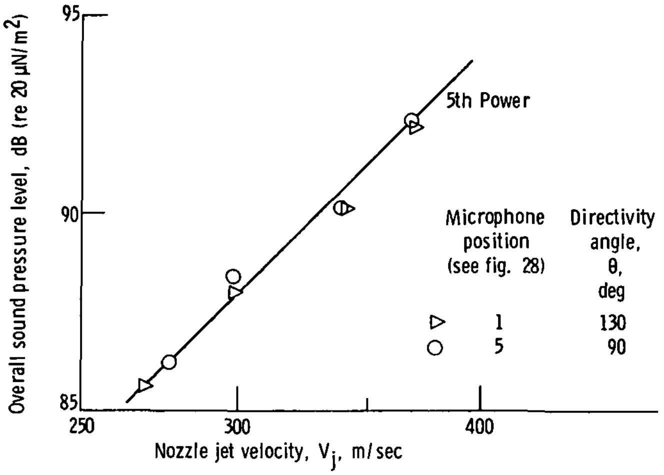

Figure 29. - Overall sound pressure level as function of nozzle jet velocity at two sideline locations for azimuthal plane angle of 27°. Augmentor setting, δ_F, 20°; lossless, free-field data at 30.5 meters; augmentor acoustically treated.

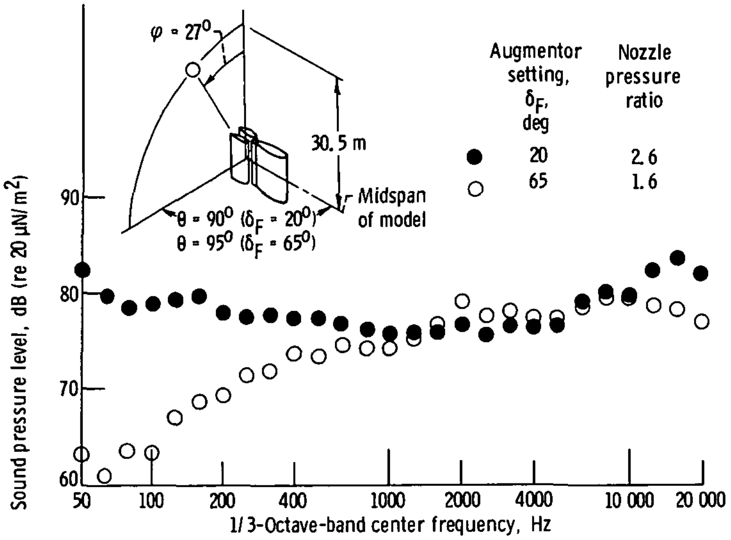

Figure 30. - Comparison of sideline 1/3-octave-band sound pressure level spectra for nominal takeoff (δ_F = 20°) and approach (δ_F = 65°) configurations. Lossless, free-field data at 30.5 meters; augmentor acoustically treated.

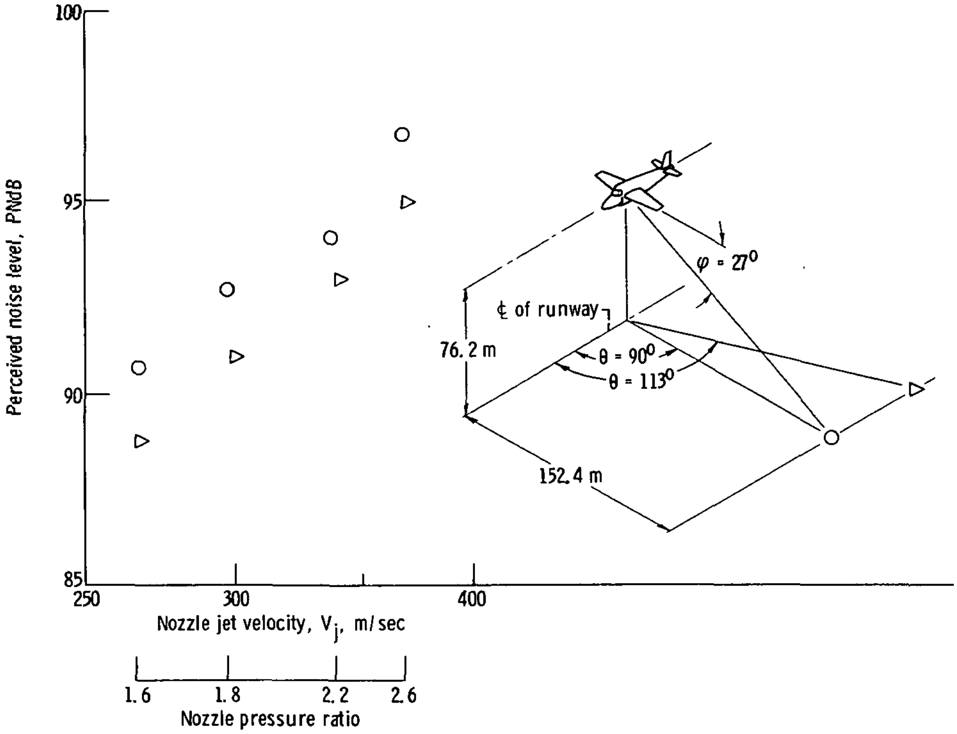

Figure 31. - Sideline perceived noise levels as function of nozzle jet velocity for a 91 000-kilogram aircraft using augmentor-wing lift augmention system. Augmentor setting, δ_F, 20^0; augmentor acoustically treated; standard day.

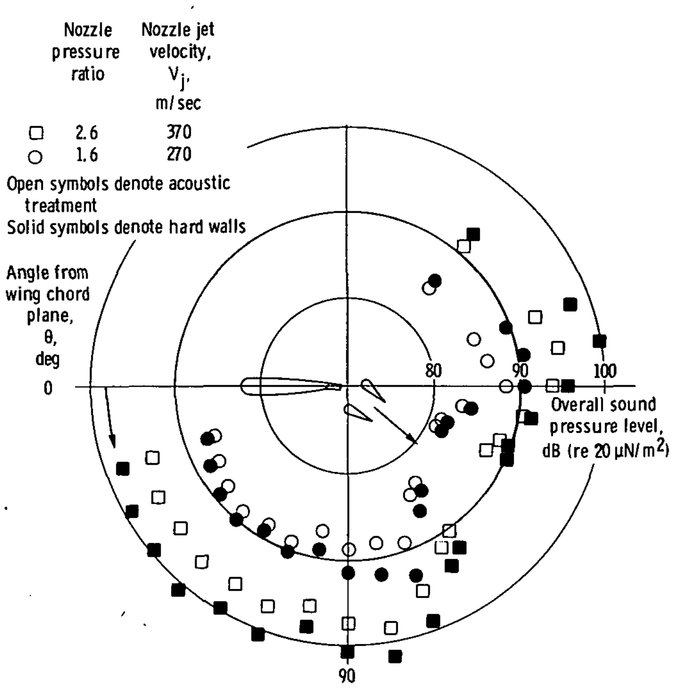

(a) Overall sound pressure level directivity patterns.

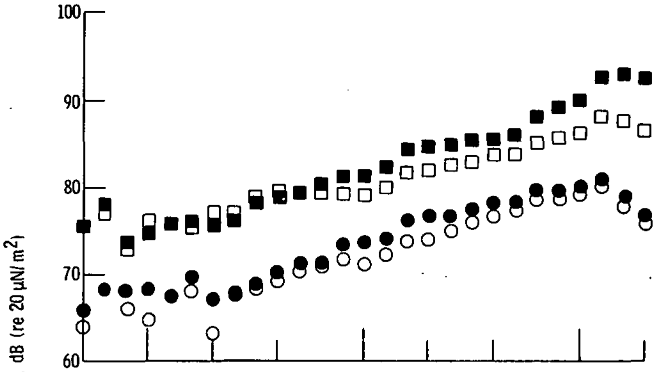

(b) 1/3-Octave-band sound pressure level at directivity angle θ of 70°.

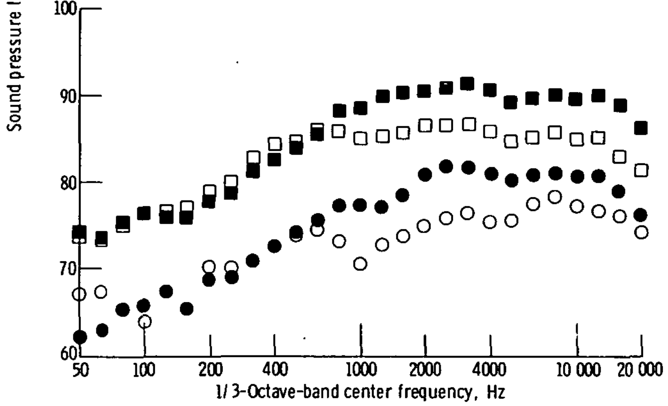

(c) 1/3-Octave-band sound pressure level at directivity angle θ of 100°.

Figure 32. - Comparison of sound levels for augmentor wing model with and without acoustic treatment. Augmentor setting, δ_F, 40°; microphone distance, 30.5 meters in flyover plane (φ = 90°).

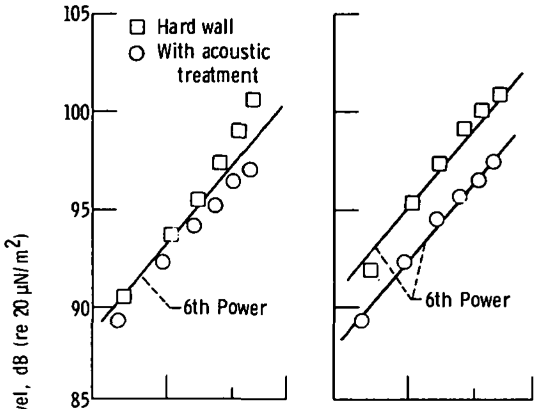

(a) Directivity angle, θ, 70°.

(b) Directivity angle, θ, 90°.

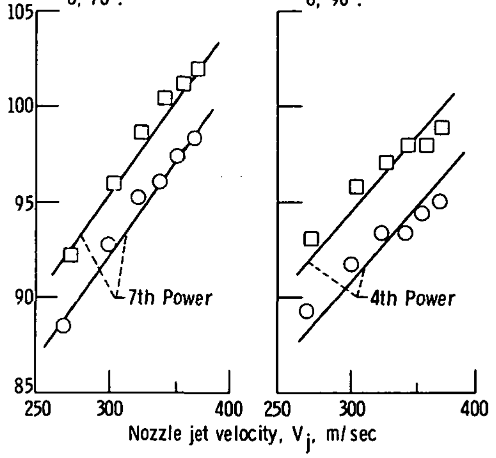

(c) Directivity angle, θ, 100°.

(d) Directivity angle, θ, 110°.

Figure 33. - Overall sound pressure level as function of nozzle jet velocity at various directivity angles. Augmentor setting, δ_F, 40°; microphone distance, 30.5 meters in flyover plane (φ = 90°).

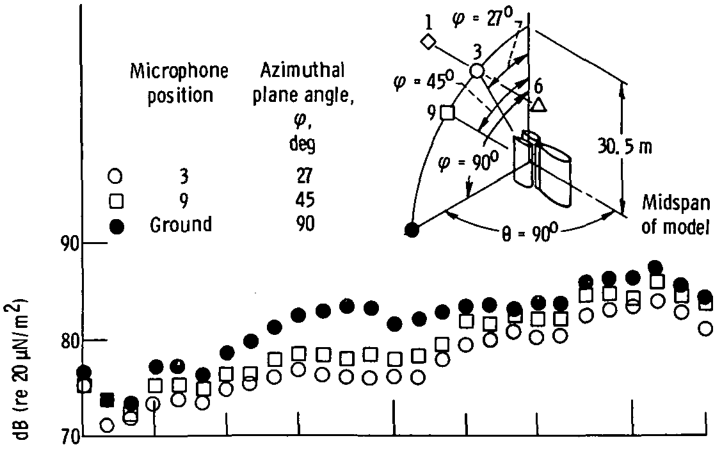

(a) Variation in azimuthal plane angle at directivity angle θ of 90°.

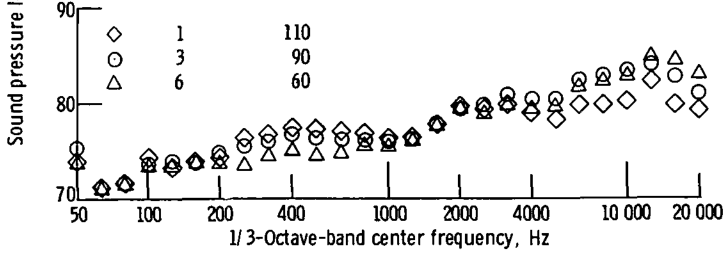

(b) Variation in sideline position at azimuthal plane angle φ of 27°.

Figure 34. - 1/3-Octave-band sound pressure level spectra at various sideline locations. Augmentor setting, δ_F, 40°; nozzle pressure ratio, 2.6; lossless, free-field data at 30.5 meters; augmentor acoustically treated.

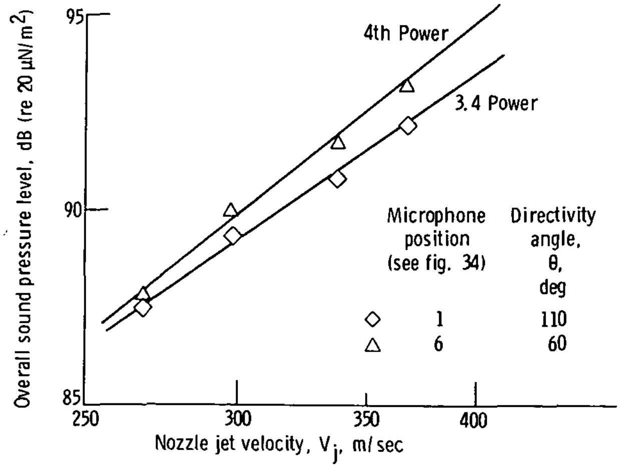

Figure 35. - Overall sound pressure level as function of nozzle jet velocity at two sideline locations for azimuthal plane angle φ of 27°. Augmentor setting, δ_F, 40°; lossless, free-field data at 30.5 meters; augmentor acoustically treated.

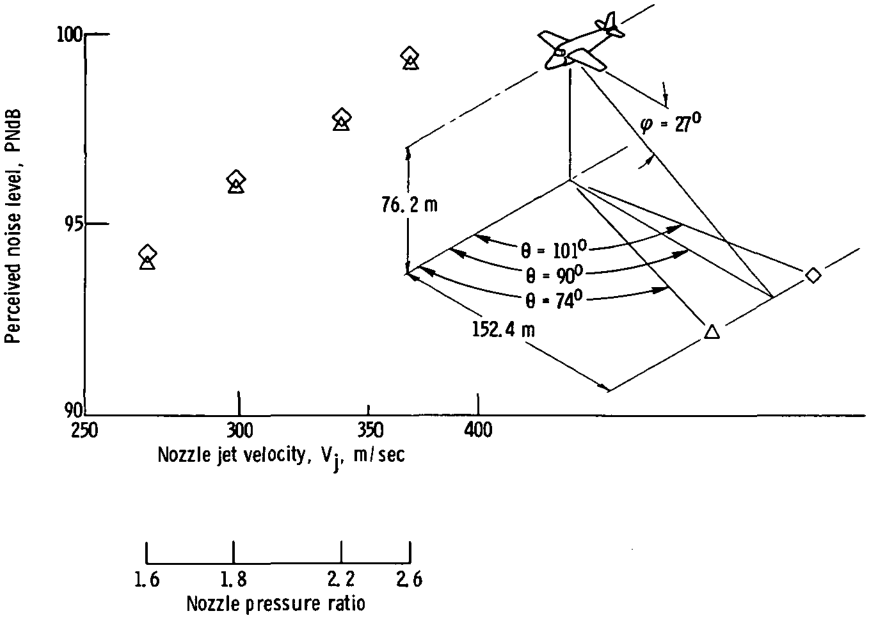

Figure 36. - Sideline perceived noise levels as function of nozzle jet velocity for 91 000-kilogram aircraft using augmentor-wing powered lift system. Augmentor setting, δ_F, 40^0; augmentor acoustically treated; standard day.

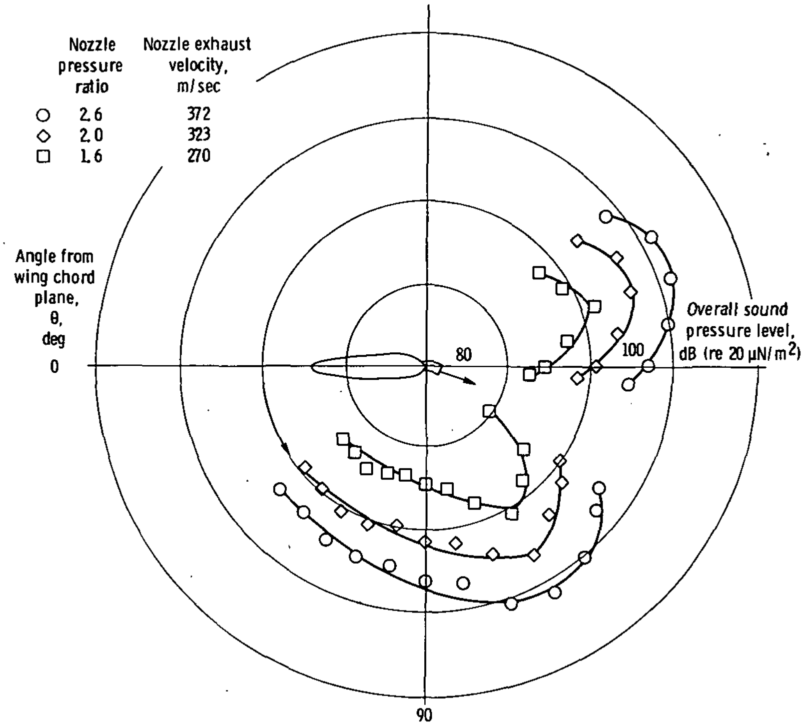

(a) Overall sound pressure level directivity patterns.

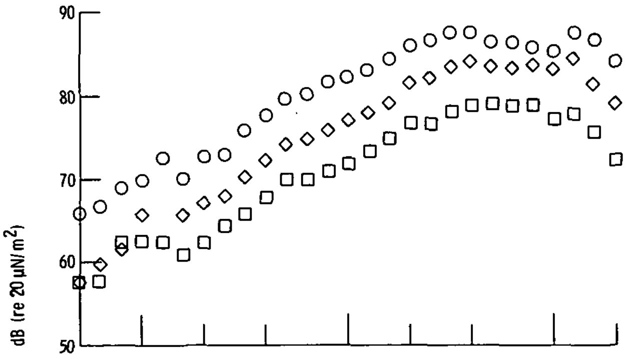

(b) 1/3-Octave-band sound pressure level spectra at directivity angle θ of 50°.

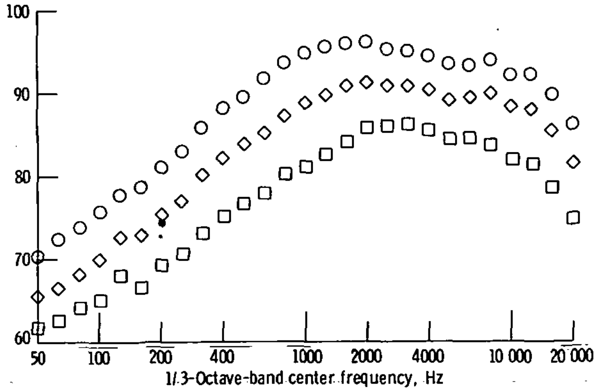

(c) 1/3-Octave-band sound pressure level spectra at directivity angle θ of 120°.

Figure 37. - Nozzle-alone sound levels as function of nozzle pressure ratio. Microphone distance, 30.5 meters in flyover plane (φ = 90°). Wing in place.

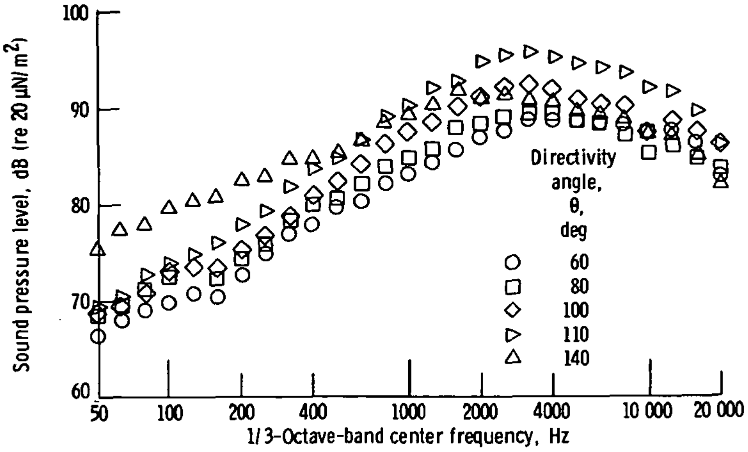

Figure 38. - Nozzle-alone 1/3-octave-band sound pressure level spectra as function of directivity angle for nozzle pressure ratio of 2.6. Microphone distance, 30.5 meters in flyover plane (φ = 90°).

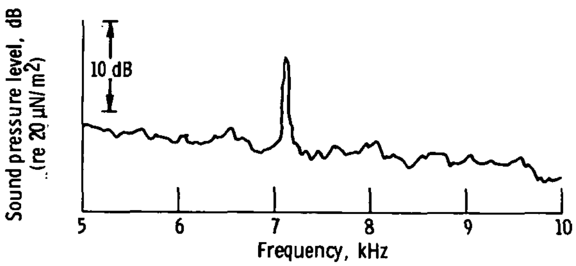

(a) Narrow-band spectrum (30-Hz bandwidth) at directivity angle θ of 50° for nozzle pressure ratio of 2.0.

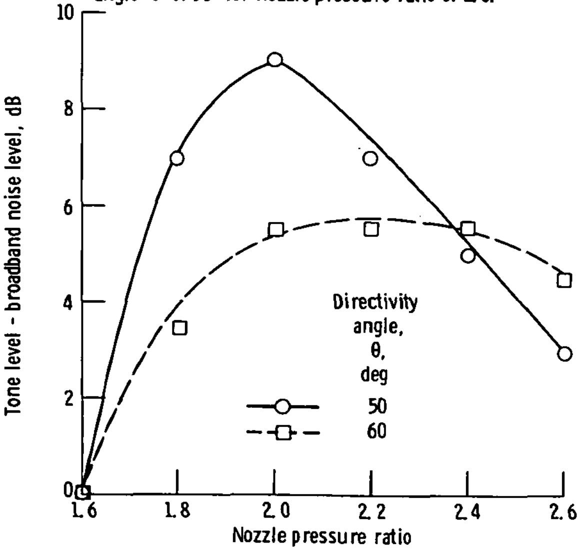

(b) Difference between tone level and broadband noise level. Frequency, 7200 hertz.

Figure 39. - Narrow-band acoustic results for nozzle alone at 30.5 meters in flyover plane (φ = 90°).

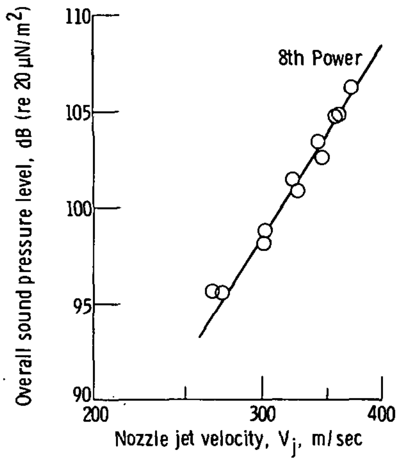

Figure 40. - Peak overall sound pressure level as function of nozzle jet velocity for corrugated-lobe nozzle alone. Directivity angle, θ, 120° (peak noise angle); microphone distance, 30.5 meters in flyover plane (φ = 90°).

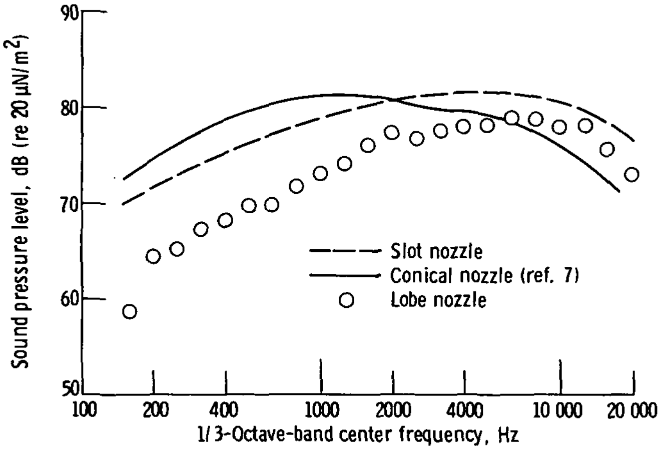

Figure 41. - Comparison of 1/3-octave-band spectra for slot nozzle, conical nozzle, and corrugated-lobe nozzle alone. Directivity angle, θ, 90° from nozzle exhaust; nozzle jet velocity, V_j, 303 meters per second; microphone distance, 30.5 meters in flyover plane (φ = 90°).

NASA-Langley, 1977 E-8923

NATIONAL AERONAUTICS AND SPACE ADMINISTRATION
WASHINGTON, D.C. 20546

OFFICIAL BUSINESS
PENALTY FOR PRIVATE USE $300

SPECIAL FOURTH-CLASS RATE
BOOK

POSTAGE AND FEES PAID
NATIONAL AERONAUTICS AND
SPACE ADMINISTRATION
451

U.S.MAIL

POSTMASTER : If Undeliverable (Section 158 Postal Manual) Do Not Return

> *"The aeronautical and space activities of the United States shall be conducted so as to contribute . . . to the expansion of human knowledge of phenomena in the atmosphere and space. The Administration shall provide for the widest practicable and appropriate dissemination of information concerning its activities and the results thereof."*
>
> —NATIONAL AERONAUTICS AND SPACE ACT OF 1958

NASA SCIENTIFIC AND TECHNICAL PUBLICATIONS

TECHNICAL REPORTS: Scientific and technical information considered important, complete, and a lasting contribution to existing knowledge.

TECHNICAL NOTES: Information less broad in scope but nevertheless of importance as a contribution to existing knowledge.

TECHNICAL MEMORANDUMS: Information receiving limited distribution because of preliminary data, security classification, or other reasons. Also includes conference proceedings with either limited or unlimited distribution.

CONTRACTOR REPORTS: Scientific and technical information generated under a NASA contract or grant and considered an important contribution to existing knowledge.

TECHNICAL TRANSLATIONS: Information published in a foreign language considered to merit NASA distribution in English.

SPECIAL PUBLICATIONS: Information derived from or of value to NASA activities. Publications include final reports of major projects, monographs, data compilations, handbooks, sourcebooks, and special bibliographies.

TECHNOLOGY UTILIZATION PUBLICATIONS: Information on technology used by NASA that may be of particular interest in commercial and other non-aerospace applications. Publications include Tech Briefs, Technology Utilization Reports and Technology Surveys.

Details on the availability of these publications may be obtained from:

SCIENTIFIC AND TECHNICAL INFORMATION OFFICE

NATIONAL AERONAUTICS AND SPACE ADMINISTRATION

Washington, D.C. 20546